Influence of grit particles characteristics on the abrasive wear micro-mechanisms of NbC-Ni and WC-Co hard materials

Naveenkumar Rajendhran[1,], Kannaki Pondicherry[1], Shuigen Huang[2], Jozef Vleugels[2], Jacob Sukumaran[1], Patrick De Baets[1,3,4]*

[1] Soete Laboratory, Department of Electromechanical, Systems and Metal Engineering, Ghent University, B-9052 Ghent, Belgium

[2] Department of Materials Engineering, KU Leuven, B-3001 Leuven, Belgium

[3] Flanders Make, The Strategic Research Centre for the Manufacturing Industry, B-3001, Leuven, Belgium

[4] Unit of Systems and Component Design, KTH Royal Institute of Technology, SE-100 44 Stockholm, Sweden

Abstract

Knowledge of wear and associated damage mechanism that is prevalent during abrasive wear conditions using NbC-based cermets is lacking. In the current investigation, the abrasive wear response and associated damage mechanisms of cermets due to characteristics effect of grit particles such as size and hardness have been explored. The present study evaluates the abrasive wear response of NbC-12Ni-10Mo_2C (NbC-Ni) cermet during two-body abrasive wear, which was experimentally simulated by a pin abrasion tester following the ASTM G132 standard. The WC-Co cemented carbide (WC-15.6Co) with similar hardness was used as a reference material in this study for a comprehensive comparison of materials. The investigated test parameters included different applied loads (4-16 N) and abrasive particle sizes (22-200 μm) for a 30 m sliding distance at 0.15 m/s sliding velocity. Silicon carbide (SiC) and aluminium oxide (Al_2O_3) were used as abrasive counter bodies. Test results clearly show the particle size effect and the critical abrasive particle size (CPS) for the cermet lies between 82 μm and 125 μm for both abrasives (SiC, Al_2O_3). It is noticed that the wear rate shows three different trends as the particle size increases, initial increase then a steady state during critical particle size and becomes unpredictable. This effect reflects the transition of wear micro-mechanisms dominated from binder removal (below CPS) to fracture and fragmentations (beyond CPS). The wear mode transition map from plastic grooving to fracture-dominated failure (fragmentation and granular cracks) was created by correlating factors such as the severity of contact and specific wear rate with microscopic observations. The wear produced by SiC abrasives was about an order of magnitude higher (≈18x) than with Al_2O_3 abrasives. In addition, the material comparison highlight that the abrasive wear rate of NbC-Ni cermet was about 37-86 % (SiC) to 66-83 % (Al_2O_3) higher than for the WC-Co cemented carbide, despite both cermets having similar micro-hardness. In addition, the present study illustrates that the abrasion of cermets is not only related to mechanical properties such as hardness and fracture toughness but is inherently related to composite chemical properties such as wettability and interfacial strength. This work provides new insight into the wear response of NbC-Ni cermets and WC-Co cemented carbides regarding different abrasive counterfaces, abrasive particle sizes and transition of abrasive wear mechanisms.

Keywords: NbC-cermet, WC-Co cemented carbide, abrasive size effect, wear micro-mechanisms

*corresponding author

Email - Naveenkumar.Rajendhran@Ugent.be

1. Introduction

Cermets are composites consisting of hard ceramic particles (carbides, nitrides and borides) bonded with soft metallic binders (cobalt, nickel, molybdenum and iron) [1]. Tungsten carbide-cobalt (WC-Co) is the most widely used cermet for cutting tools and wear parts due to its high hardness and fracture toughness [1, 2]. However, concerns over economic and environmental issues have prompted research into alternative materials [3-5]. Niobium carbide (NbC) has emerged as a promising option, offering high hot hardness and lower solubility in steels and cast iron compared to WC [6, 7]. Despite numerous studies on the microstructural and mechanical properties of NbC-cermets [8-10], the wear resistance of NbC-Ni cermets during tool wear remains largely unexplored. Earlier research on cutting tools suggests that abrasion (flank wear), adhesion (built-up edge), diffusion-dissolution (crater wear) and oxidation are the main mechanisms contributing to tool wear. Among these, the flank wear due to abrasion is often used to determine tool life, as it determines surface finish, residual stress and microstructure changes [11]. However, quantifying abrasion on a real scale is challenging, especially since multiple factors contribute during the machining (wear) process. Few experimental studies have been standardised to assess the abrasion resistance of cemented carbides and cermets on a laboratory scale, where both have advantages along with drawbacks [12]. The abrasion mechanism developed on a cutting tool is very similar to a closed two-body abrasion [13].

Appendix – I highlights the detailed literature on abrasive wear and associated micro-mechanisms of various cermets [14-33]. Above all, limited study has shown the abrasive wear behaviour of NbC-based cermets, but there was no further explanation of the wear micro-mechanisms [29]. According to the literature, the input parameters such as material properties, abrasive particle characteristics and other operating conditions are the major governing factors for inducing different micro-wear mechanisms. The mechanical properties *i.e.* hardness, fracture toughness and strength responsible for the abrasion of cermets are mainly dependent on the microstructural features such as WC grain size and binder content [34]. Additionally, the characteristics of the abrasive particles namely, hardness, size and shape as well as the operational parameters including load and sliding speed also affect the abrasion of cemented carbides [33]. It has been noted that the abrasive wear mechanism depends on the hardness ratio of the abrasive particle (H_a) and tested surface (H_s). Experimental results showed that plastic grooving is ensured on a test surface if the hardness ratio (H_a/H_s) is greater than ≈1.2 for homogenous materials, whereas for inhomogeneous materials such as cermets is around ≈1.5 [30]. Therefore, it is assumed that for cermets the abrasion under the condition where H_a/H_s <1.2 is referred to as soft abrasion, contrary to hard abrasion when H_a/H_s >1.5 [35].

Limited studies address the effect of the abrasive particle size on the wear rate of cemented carbide, without critical particle size (CPS) considerations [30, 31]. The size effect (of most metals) displayed three different trends in wear volume as the abrasive grit size increased, which increase significantly in the beginning and changed to a steady state during the critical particle size (about ≈100 µm in most literature) then it becomes independent (steady-state or decreasing or increasing) [33, 36]. Sahariah et al. [33] reported the particle size effect on the wear mechanisms transitions of WC-Co-Cr coating and concluded that the dominated wear mechanisms shift from fatigue and plastic deformation to fracture and fragmentation as the particle size increases and the CPS was noticed around ≈100 µm. A recent study on pin abrasion test for WC-Co showed that the dominant wear mechanism changed from binder removal to fracture and fragmentation as the SiC grit size changed from small (21.8 µm) to large (125 µm), but the observed particle size effect was not discussed [37]. To overcome this inadequacy, it is necessary to assess the abrasive wear rate with different abrasive particle sizes ranging from fine to coarse for both WC-cemented carbides and NbC based cermets.

The present study aims at investigating the wear of two comparable micro-hardness, WC-cemented carbide (reference) and NbC-cermet (test material) from the viewpoint of two-body abrasive wear. Besides, the effect of abrasive particle characteristics such as size and hardness on the micro-wear mechanisms of hard materials has been explored.

2. Experimental

2.1. Pin abrasion tester (ASTM G132 test rig)

In this study, a pin abrasion tester was selected to experimentally simulate the two-body abrasion according to the ASTM G132 standard (see **Fig. 1**). The disc containing adhesive grit paper rotates against the pin which is mounted on the loading arm moves in the horizontal direction. This results in a spiral sliding path and ensures that the specimen is continuously in contact with fresh abrasives simultaneously. The coefficient of friction of the test pair was computed based on the tangential force measured by the load sensor. The abrasive wear rate (*AWR*) and specific wear rate (K) of the test sample was calculated using Archard's wear relation;

$$AWR = \frac{V}{S} \qquad (\text{mm}^3/\text{m}) \qquad (1)$$

$$K = \frac{V}{P.S} \qquad (\text{mm}^3/\text{N-m}) \qquad (2)$$

where, V = material volume loss calculated from the ratio of mass loss to material density (mm^3), S = sliding distance (m), and P = normal load (N).

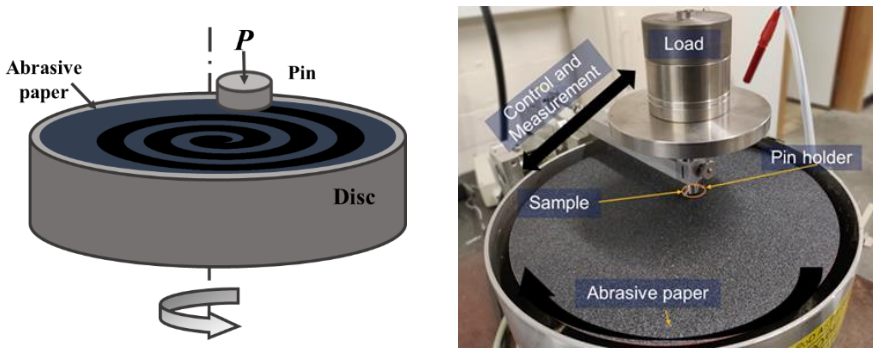

Fig. 1. Schematic (left) and photograph (right) of the pin abrasion tribo-tester.

2.2. Materials

The as-sintered NbC-Ni cermet (NbC-12Ni-10Mo_2C) and cemented carbide (WC-15.6Co) used as test and reference material, respectively, were supplied by the Department of Materials Engineering of KU Leuven, Belgium. The comprehensive material preparation and microstructural characteristics of these sintered carbides have been reported elsewhere [38]. The WC-Co pins used in this study were purchased from Tongda cemented carbide, a commercial supplier based in China. NbC (FSSS≈1.52 µm, CBMM, Brazil), Mo_2C (FSSS≈3.50 µm, Langfeng, China) and Ni (FSSS≈3-7 µm, Vale, T123TM, UK) powders were used to prepare the NbC-Ni cermets. The NbC powder has a total C and O content of 11.2 and 0.17 wt% respectively. To prepare the NbC matrix cermets, a powder mixture of NbC-12Ni-10Mo_2C (vol%) was mixed in ethanol using a multi-directional mixer (Turbula, WAB, Switzerland) for 48 hours. The milling balls used were WC-6 wt% Co (Ceratizit grade H20C) with a diameter of 10 mm. The dried powder was cold isostatically pressed at a pressure of 200 MPa using EPSI equipment. The resulting powder compacts were subsequently pressureless sintered in a graphite furnace under vacuum conditions (≈20 Pa) at a heating rate of 5 °C/min. The sintering process lasted for 60 minutes at a temperature of 1420 °C.

The chemical composition and mechanical properties of both materials are given in **Table 1**. The density of the sintered cermets was measured in ethanol by the Archimedes method. The average grain size of the carbide grains was measured using the line intercept method on back-scattered electron images, without applying a correction factor [39]. The Vickers hardness (HV_{30}), was measured (Model FV-700,

Future-Tech Corp., Japan) with an indentation load of 294 N for 15 s at room temperature. The Palmqvist indentation fracture toughness (K_{1C}), was calculated based on the length of the radial cracks around the Vickers indentations, using the formula proposed by Shetty *et al.* [40]. The room temperature flexural strength was measured in a three-point bending test (Instron 4467, PA, USA) on rectangular samples (25x 3x 2 mm), with a span length of 20 mm and a cross-head displacement of 0.1 mm/min. The elastic modulus (E) was measured on rectangular bars using the resonance frequency method. The resonance frequency was obtained using the impulse excitation technique (Grindo-Sonic, J.W. Lemmens N.V., Leuven, Belgium). The reported values for hardness, fracture toughness, and flexural strength represent the mean and standard deviation of five measurements.

Table 1. Properties and composition of the hard materials

Hard materials	**Unit**	**WC-Co**	**NbC-Ni**
Composition	Vol %	WC-15.6Co	NbC-12Ni-10Mo_2C
	wt%	WC-9.5Co	NbC-13.3Ni-11.2Mo_2C
Density	g/cm³	14.62 ± 0.02	8.06 ± 0.03
Hardness (HV_{30})	kg/mm^2	1383 ± 18	1348 ± 3
Fracture toughness (K_{1C})	MPa m$^{1/2}$	10.9 ± 0.6	8.29 ± 0.1
Flexural strength	MPa	2900 ± 100	1568 ± 44
E-modulus	GPa	540 ± 10	440 ± 20
Poisson ratio	-	0.31 ± 0.02	0.25 ± 0.02
Aver. carbide grain size	μm	1.56 ± 0.72	2.14 ± 0.6
Thermal conductivity [41, 42]	W/m-K	29.2	14.2
Roughness	μm	0.1 ± 0.02	0.1 ± 0.02

2.3. Surface topography and morphology

The surface topography of the contact surfaces was characterized by Taylor Hobson CCI-HD white light interferometer followed by the ISO 13565-2 standard. The test pins (surfaces) used in this study are electrical discharge machined (EDM) and ground to an average surface roughness of 0.1 ± 0.02 μm. In order to check the microstructure morphology, the following metallography procedure has been utilised. The first step involves preparing the mounting, wherein the samples are embedded in PolyFast resin using a hot compression press at 180°C for curing times of 5 minutes of heating and 3 minutes of fast cooling using ProntoPress-20 (Struers, Denmark). Subsequently, surface grinding is performed with caution using a Tegramin-20 grinding machine (Struers, Denmark). The mechanical preparation can be divided into two stages, namely grinding and polishing. The appropriate grinding disc and polishing cloths were selected based on the polishing guide from Struers, to achieve a mirror-like surface finish. **Table 2** outlines the metallography procedures and test conditions followed during the grinding and polishing of the carbide specimens.

Table 2 Matalog guide/procedure.

Procedure	**Polishing pad**	**Suspension**	**Grain (μm)**	**Load (N)**	**Speed (rpm)**	**Time (min)**
Plane grinding	MD-Piano 200	Water	-	180	300	Until plane
Fine grinding	MD-Allegro	DP suspension	9	210	150	4
Polishing	MD-Dac	DP suspension	3	180	150	6
	MD-Chem	OP-S suspension	-	90	150	2

The microstructure of the WC-Co and NbC-Ni cermet was characterized through SEM-FEG (JEOL JSM-7600F). The integrated EDS-energy dispersive X-ray spectroscopy X-Max (Oxford instruments, UK) was used to quantify the elemental analysis and mapping on the hard material surfaces and countersurface before and after the test. In **Fig. 2a and b**, the dark interconnected phase represents the metal binder (Co, Ni) whereas the bright contrast skeleton corresponds to the carbide phase (WC, NbC). In **Fig. 2b**, the small residual pores or impurities of oxides, specifically NbC_xO_y or NbO_z, are observed as submicron black intergranular spherical spots [10]. The sintered carbide particles typically exhibit a faceted shape, but some of the smaller NbC grains appear spherical, and the corners of NbC grains in larger grains are slightly rounded. This suggests that the thermodynamic stability of the solid solution phase increased with the addition of Mo_2C [38]. The Mo_2C addition is dissolved in both the carbide and binder phases, while the Mo content in the (Nb,Mo)C carbide phase is relatively lower compared to the Ni(Mo) binder phase [38]. **Fig. 2c and d** show the area analysis (30 x 20 µm) EDS spectra of the various elements on the pristine WC and NbC hard materials surface obtained from the EDS mapping.

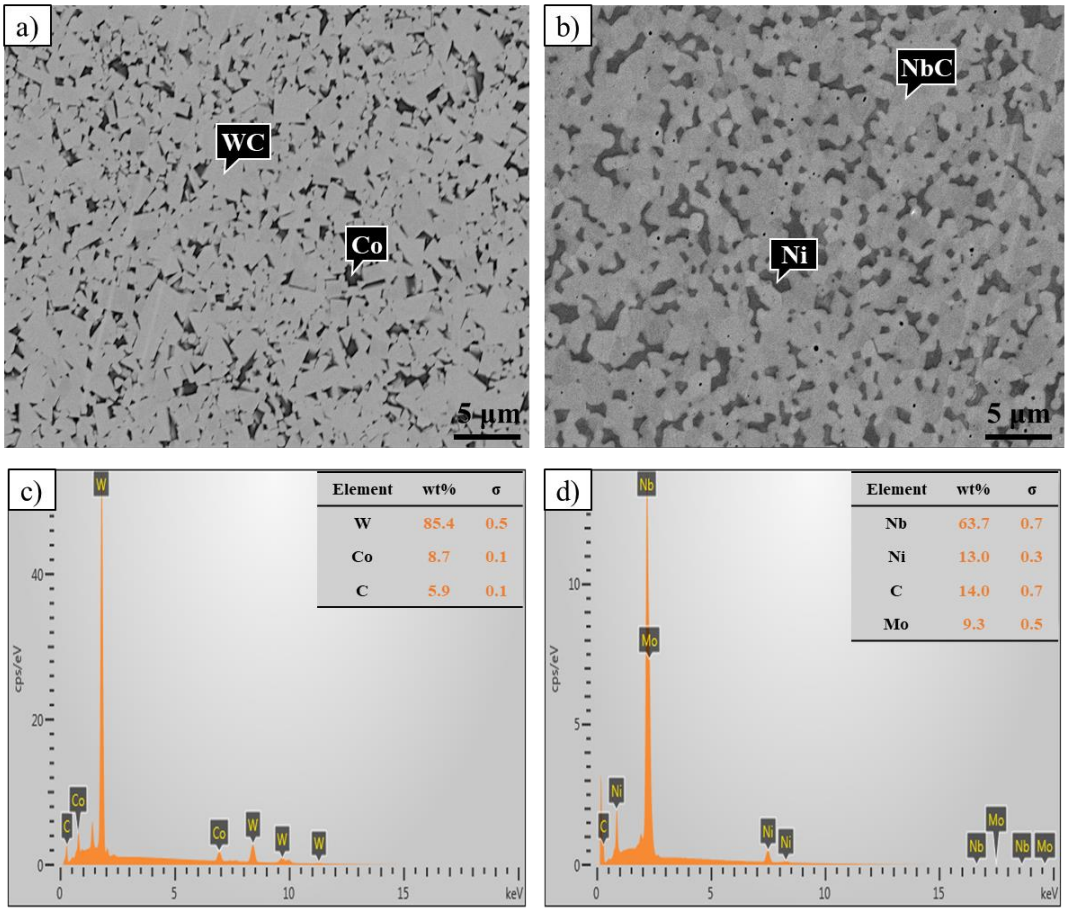

Fig. 2. Backscattered SEM and EDS spectra of the (a and c) WC-Co and (b and d) NbC-Ni hard materials. Note: Carbon (C) value is only qualitative.

2.4. Experimental testing

The test sample was a cylindrical pin with a length of 5 mm and a diameter of 8 mm and the contact surfaces were machined by EDM (electrical discharge machining) and grounded. The test loads, from 4 to 16 N, were applied using calibrated dead weights. Two types of FEPA grade abrasive papers (Struers GmBH and QATM-Metallography, EU) were used in this operation, namely SiC (α-SiC) and Al_2O_3 (α -Al_2O_3), with different grit sizes: P800, P180, P120 and P80 with their respective particle sizes of 22 µm, 82 µm, 125 µm and 200 µm. A total sliding distance of 30 m was imposed at a constant rotation speed

(sliding speed) of 0.15 m/s. The tests were performed at room temperature of 24 ± 0.5°C and the relative humidity was maintained at about 45-55 % during all the experiments. The tests were performed performed in dry abrasive wear conditions and each test was repeated three times to check repeatability. The samples were thoroughly cleaned using ultrasonic cleaning in acetone for 10 minutes before and after the test. The samples were weighed using an electronic balance with an accuracy of ± 0.1 mg before and after the test to obtain the mass lass.

2.5. Grit particle characterisation

SEM observation showed the characteristics of the abrasive particles by size and shape to identify parameters that influence their abrasivity (see **Fig. 3**). Despite the similar size, the SiC particles have a higher angular shape (sharp edges) than Al_2O_3 abrasive particles. The shape of the Al_2O_3 abrasives varied from a sharp point to rounded edges as the particle size increased. Literature reported that the particle abrasivity is increased as the circularity decreases [43]. The surface height and shape parameters such as maximum profile height (S_z) and the circularity index (F_a) of grit particles were analysed through KEYENCE optical profilometry (VR-5000, Japan) and tabulated in **Table 3**. This further justifies the aforementioned SEM observation that an increase in particle size increases the circularity of both SiC and Al_2O_3 grits, also the circularity index of Al_2O_3 was relatively high compared to SiC despite the similar particle size. The maximum profile height (S_z) for SiC and Al_2O_3 abrasives is different since the SiC particle shape is sharper (more angular) than the alumina grit which has slightly rounded corners. The maximum profile height (S_z) of the grit papers in this study includes the height of the grit particles and the transparent resin coating that holds the grits in place. In this case, a transparent resin is used to cover the abrasives and secure them to the paper. The difference in the maximum profile height can be attributed to the fact that the surface is unfiltered. When measuring the surface, it was not possible to clearly distinguish between the resin and the particles, since the resin is transparent. Hence, without proper identification of the reference plane, it was not possible to proceed with the normalization of the surface. To conclude, the assessed maximum profile height (S_z) encompasses both the particles and the transparent resin, which explains the higher values found in comparison to the mean particle size. The comprehensive mechanical and thermal properties of SiC and Al_2O_3 abrasives have been gathered from the abrasives supplier and literature [41, 44]. The properties are summarised in **Table 4**.

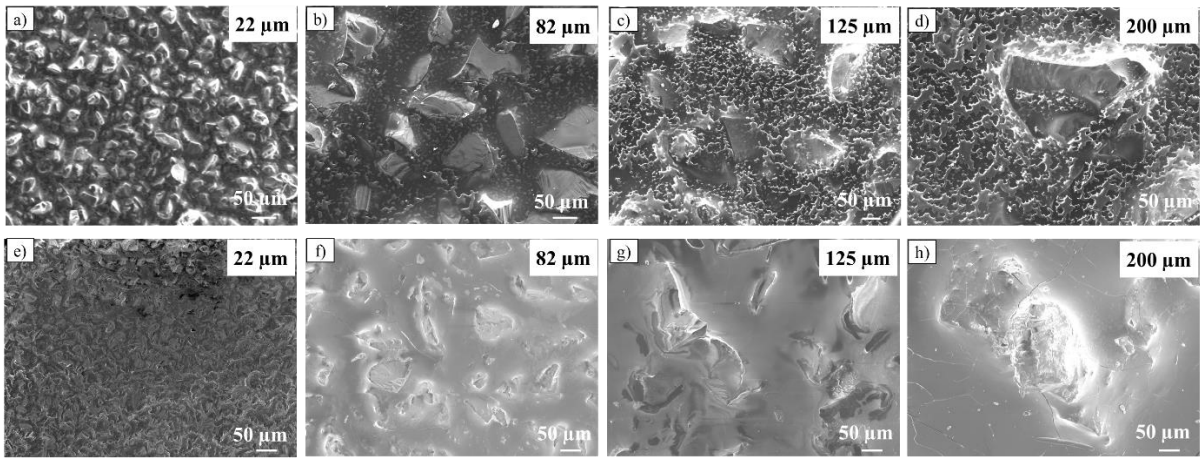

Fig. 3. SEM images of pristine SiC (a-d) and Al_2O_3 (e-h) abrasives with different particle sizes from 22 µm to 200 µm.

Table 3. Abrasive particle characteristics.

FEPA Grit	Particle size [µm]	Apex angle (2θ) [°]	Maximum profile height (S_z) (mm)		Circularity	
			SiC	Al_2O_3	SiC	Al_2O_3
P800	22	90	0.07	0.06	0.32	0.36
P180	82	111	0.41	0.21	0.41	0.54
P120	125	117	0.58	0.35	0.44	0.61
P80	200	125	0.68	0.42	0.49	0.71

Table 4. Mechanical and thermal properties of the abrasive grit particles.

Property	Unit	SiC	Al_2O_3
Hardness	GPa	26.4 ± 2.6	19.5 ± 1.5
Fracture toughness	MPa $m^{1/2}$	4.3 ± 2.5	3.5 ± 1
E-modulus	GPa	475	400
Poisson ratio	-	0.14	0.23
Thermal conductivity	W/m-K	41	30
Coefficient of thermal expansion	10^{-6}/°C	5.12	8

2.6. Contact pressure

The nominal contact pressure was calculated based on a pin-on-plane configuration to be between 0.1 MPa and 0.32 MPa. To calculate the real contact pressure on the real area of contact, it is important to calculate the number of particles of the grit surface located under the total area of contact. The number of particles in real contact n is calculated analytically according to Wang *et al.* using equations (3-5); [45]

$$n = \left(\frac{6NPD^{-2}}{\pi H tan^2\theta}\right)^{\frac{1}{2}} \quad (3)$$

$$N = \frac{kA}{D^2} \quad (4)$$

$$A = \pi R^2 \quad (5)$$

where n is the real number of particles in contact, N is the number of particles in the nominal contact area, D is the size of the abrasives (µm), P is the applied load (N), A is the nominal contact area (mm^2), R is the pin radius (4 mm), k is the constant ≈ 0.47 (obtained experimentally in [45] for a range of abrasive mesh sizes from 600 to 150) and θ is the half angle of the apex (°).

The nominal contact area represents the overall contact area at the macro-scale, encompassing both the actual/real contact area (where the abrasive particles make direct contact with the pin) and the non-contact regions (where there is no contact between the particles and the pin). The apex angle of the particles was obtained from a previous study [46]. The apex angle for the different abrasive grits is presented in Table 3. **Appendix – II** shows a detailed table demonstrating the number of particles on the nominal contact and real contact area, along with the corresponding calculated contact pressure for both WC and NbC cermets. The Hertz contact pressure for different particle sizes for a single grit particle is shown in **Fig. 4a**. The increasing particle size lowers the contact pressure due to the larger contact area. This is different than for a contact with multiple asperities where the contact pressure is distributed along all the asperities involved in the total contact area. **Fig. 4b** shows the contact pressure for multiple SiC grit particles on WC and NbC surfaces involved in the real area of contact at a load of 16 N. The

results show that the multi-asperity contact pressure for the real area of particles in contact is increasing as the particle size increases and the trend is logarithmic. It should be noted that the NbC-Ni and WC-Co materials exhibited a similar contact pressure for all particle sizes, with the NbC-Ni cermet generating a slightly higher pressure than the WC-Co. The coefficient of variation, calculated using the standard deviation of the elastic modulus and Poisson ratio of cermets and the variation between the contact pressures is < 1%.

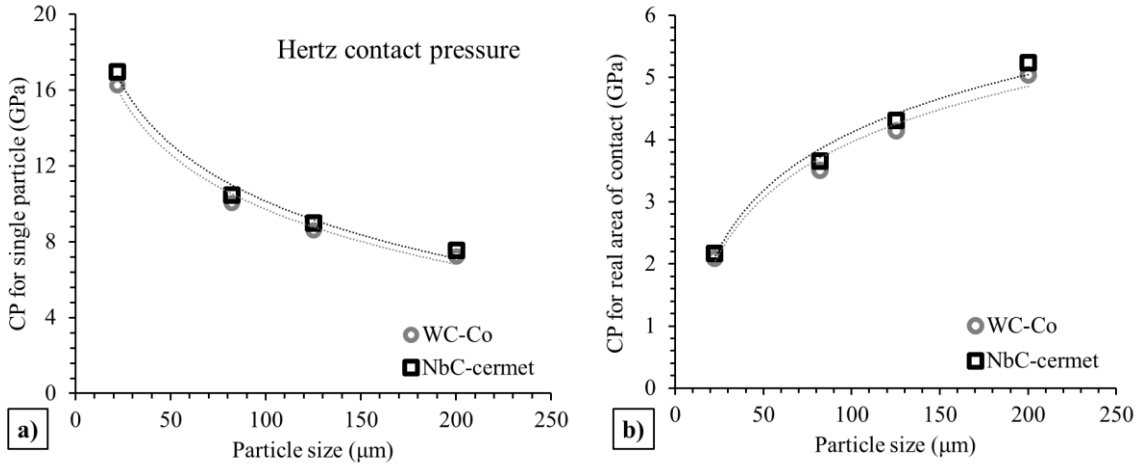

Fig. 4. Hertz contact pressure for (a) a single abrasive particle and (b) particles in a multi-asperity contact.

3. Results

3.1. Wear test result

3.1.1. WC-15.6Co cemented carbide

The abrasive wear rate (AWR) of WC-Co is plotted as a function of load and abrasive particle size against SiC and Al_2O_3 abrasives in **Fig. 5a-b** and **Fig. 5c-d**. The wear rate shows an increasing trend with increasing load and abrasive particle sizes (**Fig. 5a-b**. It is evident from **Fig. 5a**, that the regression of plots for all four particle sizes (22 µm -200 µm) remained approximately constant. It is clearly noticed that the wear rate for SiC particle shows a linear trend respective to the load, whereas the particle size produced a logarithmic trend. The measured wear rate using SiC abrasives was substantially higher than for Al_2O_3 abrasives. For example, the abrasive wear rate for fine abrasives (22 µm) was respectively 68 % (4 N) and 92 % (16 N) lower in the case of Al_2O_3 abrasives compared to SiC abrasives. For coarse particles (200 µm), the wear rate was 92 % (4 N) and 94 % (16 N) lower. Therefore, given the higher wear rate produced by SiC compared to Al_2O_3 grit paper, it is concluded that the abrasive hardness plays a major role in the abrasive wear rate. The effect of the abrasive particle size on the abrasive wear rate of WC-Co at different loads (4-16 N) for both SiC and Al_2O_3 abrasives, is shown in **Fig. 5c and d**. The abrasive wear rate increased by an order of magnitude when the particle size increased from 22 to 200 µm for SiC abrasives. However, the abrasive wear rate observed for Al_2O_3 abrasives only slightly increased with particle size along with a relatively large standard deviation (**Fig. 5d**). The wear rate for both SiC and Al_2O_3 abrasives increased from 22 µm approximately up to 100 µm and remained constant at higher abrasive particle sizes.

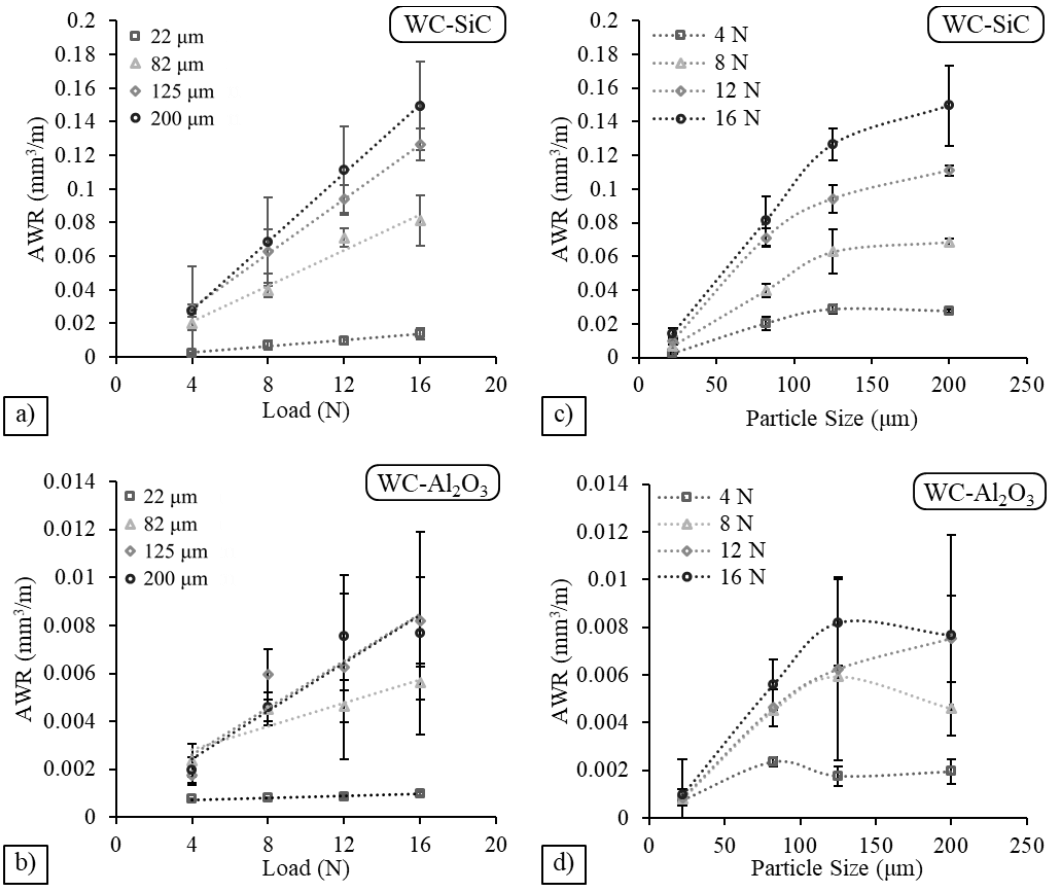

Fig. 5. Abrasive wear rate of WC-Co as a function of (a,b) load and (c,d) abrasive particle size for SiC (a,c) and Al_2O_3 (b,d) abrasives.

3.1.2. NbC-12Ni-10Mo$_2$C cermet

The influence of load and SiC and Al_2O_3 abrasive particles size on the abrasive wear rate of the NbC-Ni cermet is summarised in **Fig. 6a-d**. The abrasive wear rate generated by SiC abrasives is an order of magnitude higher than that of Al_2O_3 abrasives, indicating the abrasives hardness effect. **Fig. 6a-b** show a linear increase in abrasive wear rate of NbC-Ni with increasing system load for both abrasive counter surfaces (SiC and Al_2O_3). For SiC abrasives, the wear trend showed three different transitions with increasing particle size, i.e. a rapid increase between 22 µm and 82 µm, a steady-state between 82 µm and 125 µm, and a gradual increase above 125 µm (**Fig. 6c**). In contrast, the abrasive wear rate of NbC-Ni against Al_2O_3 abrasives showed a significant increase of approximately 125 µm particle size (**Fig. 6d**). Despite their similar hardness, NbC-Ni showed an increased abrasive wear rate of 10-38 % (SiC) and 1-64 % (Al_2O_3) compared to WC-Co. This illustrates the fact that similar hardness hard materials do not necessarily have similar abrasive wear resistance. Hence, micro-hardness cannot be considered as the only relevant characteristic to evaluate the abrasive wear of cemented carbides and cermets.

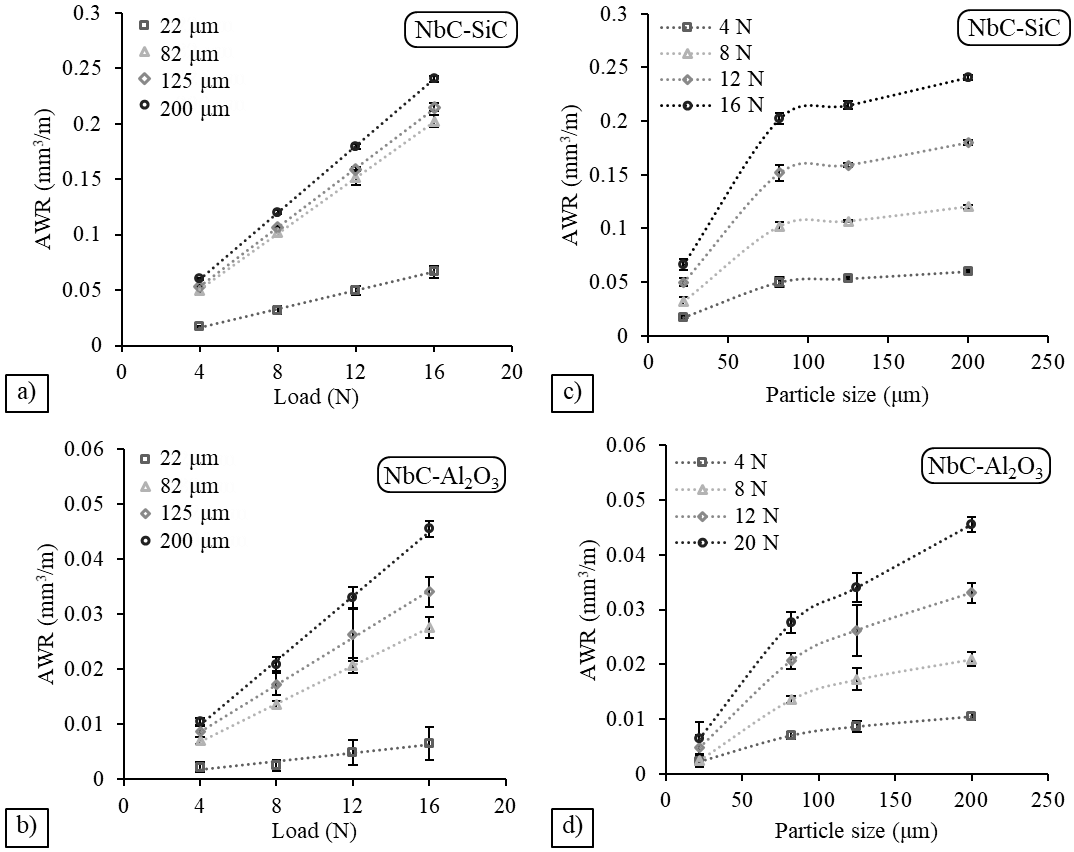

Fig. 6. Abrasive wear rate of NbC-Ni as a function of (a,b) load and (c,d) abrasive particle size for SiC (a,c) and Al_2O_3 (b,d) abrasives. Note: The error bars for SiC are not visible clearly because the coefficient of variation is ≤ 8%.

3.2. Worn surface characterisation

3.2.1. WC-15.6Co cemented carbide

Fig. 7a-h compares the SEM micrographs of WC-Co worn surfaces against SiC and Al_2O_3 abrasives. Surface deformation by plastic grooving increased with increasing particle size for both abrasives. The wear micro-mechanism observed with 22 µm SiC abrasives was mainly binder removal accompanied by micro-fracture of the carbide grains (inset **Fig. 7a**). The binder is removed by repeated plastic

deformation and micro-grooving mechanisms. At 16N load and 22 µm SiC, the surface shows additional damage effects such as WC carbide cracking and grain pull out but the predominant wear mechanism remains binder removal. This indicates that the wear mechanism is hardly influenced by the system load when the abrasive particle size is small. Relatively, Al_2O_3 abrasives showed mixed micro-fracture and binder depletion as initial wear mechanisms for 22 µm particles (**Fig. 7e**). The degree of damage produced by Al_2O_3 abrasives is comparatively less as produced by SiC abrasives and the surface grooves produced from the abrasive particles are barely visible. Intermediate particle sizes of 82 µm and 125 µm show mixed carbide and binder extrusion as the predominant wear mechanism. Additional mechanisms such as grain pull out, grain fragmentation and carbide grain debris embedment (inset **Fig. 7c** shows the backscatter electron image) in the grooves were also observed (**Fig. 7b and c**). The plastic grooves are considerably wider and few fragmented carbide grains were present on the groove ridges. On the other hand, the Al_2O_3 abrasives of intermediate size (82-125 µm) show mixed micro-fracture and binder depletion wear mechanisms. In addition to the binder depletion, small pits were visible at several locations with intergranular facets (**Fig. 7f and g**). The worn surface with coarse (200 µm) Al_2O_3 shows severely fragmented WC grains. It is clear that the wear mechanism caused by the abrasive particles shifts from binder extrusion due to plastic grooving to a fracture dominated mechanism as the particle size increases from 22 µm to 200 µm. The overall wear mechanism was found to be fracture and fragmentations of WC grains. Moreover, repeated sliding caused a wear debris layer that is gradually embedded in the surface groves, as shown in **Fig. 7d**. WC grain fragmentation was the predominant wear mechanism with 200 µm Al_2O_3 (**Fig. 7h**).

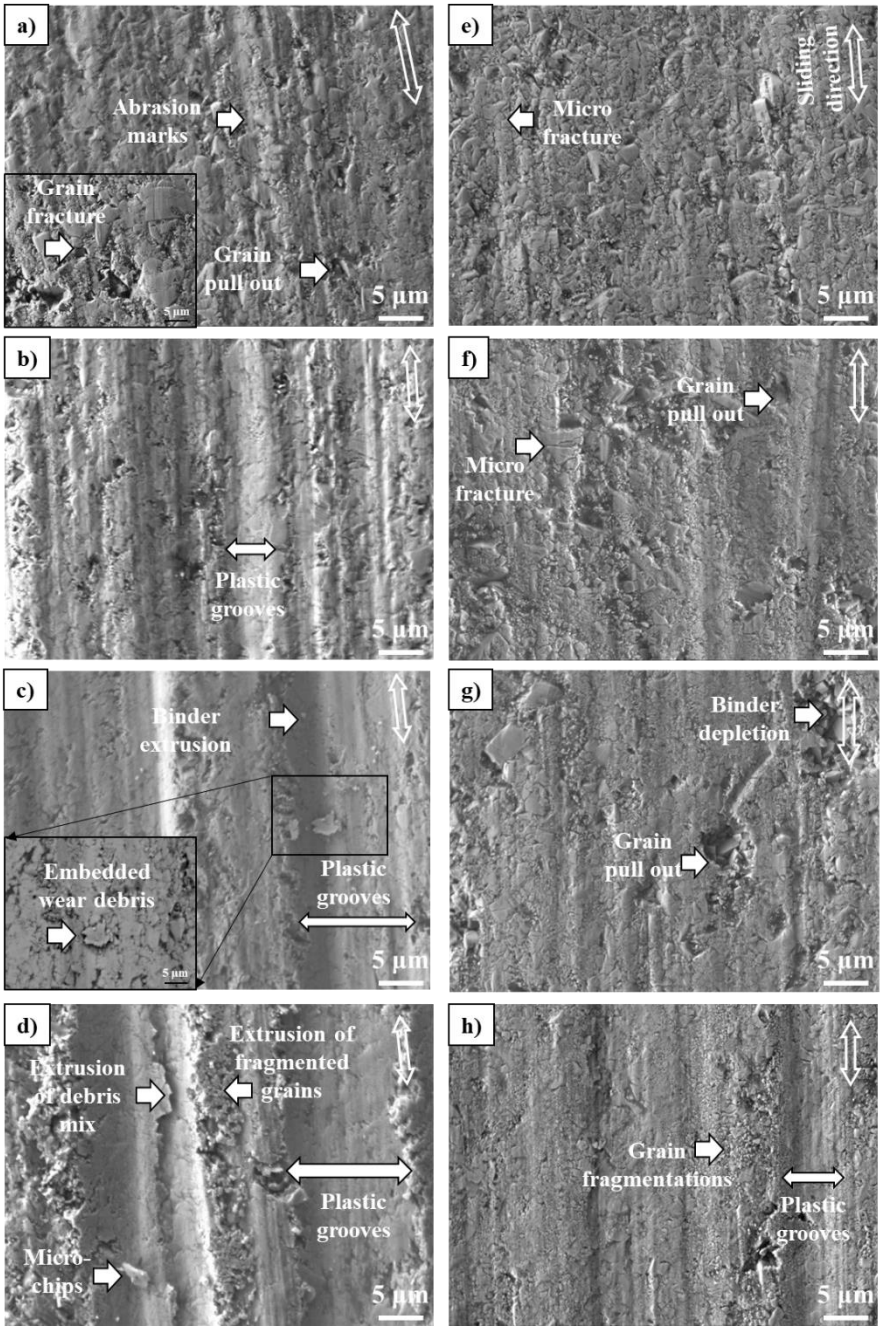

Fig. 7. SEM micrographs of WC-Co samples abraded with (a-d) SiC and (e-h) Al_2O_3 abrasives. The applied loads and corresponding abrasive sizes for each panel are as follows: (a,e) 4 N with 22 µm; (b,f) 8 N with 82 µm; (c,g) 12 N with 125 µm; and (d,h) 16 N with 200 µm.

3.2.2. NbC-12Ni-10Mo$_2$C cermet

An increase in SiC abrasive particle size tends to produce larger grooves on the NbC-Ni surface, which is evident from **Fig. 8a-d**. The worn surface of NbC-Ni against fine SiC abrasives (22 µm) indicates binder extrusion followed by micro-ploughing (**Fig. 8a**). Intermediate SiC sizes of 82 µm and 125 µm shifted the wear mechanism from micro-ploughing to fracture and fragmentation. With 200 µm SiC, the abrasion marks are wider and dominated by fracture and fragmentation of carbide grains. Furthermore, a wear debris layer was formed on the grooves with 200 µm SiC abrasives (**Fig. 8d**). This debris layer is formed due to the mechanical mixing of carbide fragments and subsequent re-embedding into the binder. On the other hand, Al_2O_3 abrasives with a particle size of 22 µm resulted in a depletion of binder

phase around the carbide grains and cavity formation indicated the evidence of carbide pull-out (**Fig. 8e**). However, the grooves formed by Al_2O_3 abrasives (**Fig. 8e**) show a lower degree of penetration than SiC abrasives (**Fig. 8a**). Despite the same load and particle size, it is noticed that the hardness of the abrasive particles strongly affects the wear mechanisms. Furthermore, the NbC-Ni surfaces experienced micro-cracking and fragmentation as an additional material removal mechanism for 82 µm (**Fig. 8f**) and 125 µm (**Fig. 8g**) Al_2O_3 abrasives. With 200 µm Al_2O_3, the damage is caused by micro-fracture and grain pull out along with binder removal/extrusion. The results show that the increment in the load results in a high degree of plastic grooves which initiates the removal of unsupported carbide grains in the NbC-Ni cermet surface.

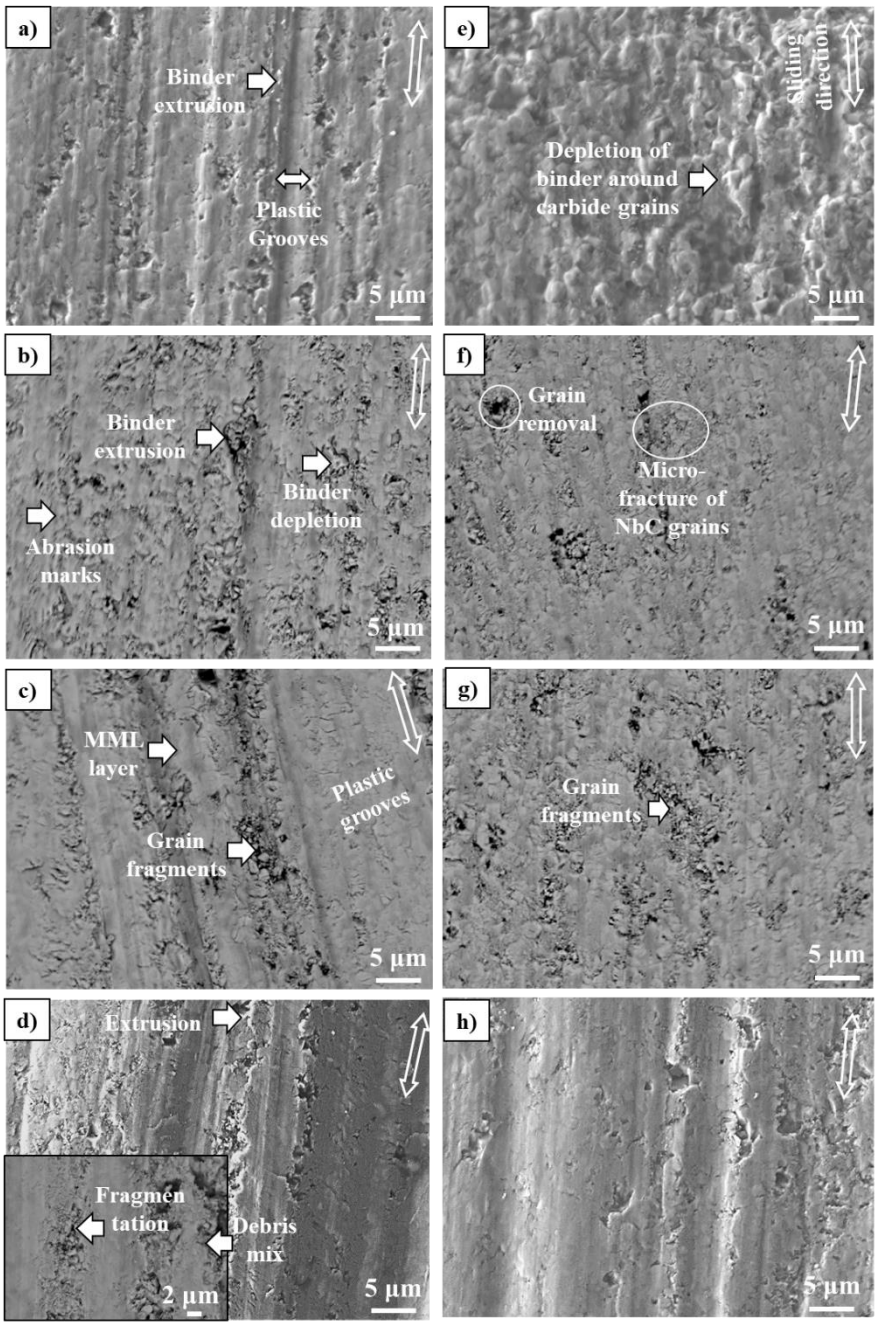

Fig. 8. SEM micrographs of NbC-Ni samples abraded with (a-d) SiC and (e-h) Al_2O_3 abrasives. The applied loads and corresponding abrasive sizes for each panel are as follows: (a,e) 4 N with 22 µm; (b,f) 8 N with 82 µm; (c,g) 12 N with 125 µm; and (d,h) 16 N with 200 µm.

3.3. 3D surface topography

The surface roughness (S_a) from 3D surface topography emphasizes the effect of different abrasives (SiC, Al_2O_3) for both WC-Co and NbC cermets, as shown in **Fig. 9**. The arithmetic mean deviation (S_a) slightly changes as a consequence of increasing load, implying the abrasive particle size has a greater influence on the S_a roughness. Both hard materials show similar S_a values for the SiC abrasive and the trend shows a logarithmic increase with the particle size, confirming the particle size effect. On the other hand, the test surface shows relatively low S_a that hardly changes with the grit size for Al_2O_3 abrasives. The observed trend with the Al_2O_3 abrasives is linear. The substantially lower S_a of the Al_2O_3 versus SiC grit indicates the hardness effect of the abrasives.

In addition to the surface roughness, the functional parameters such as peak material volume (V_{mp}) and valley void volume (V_{vv}) were also calculated from the surface material ratio curve (**Appendix - III**) obtained by the optical interferometry according to the ISO 13565-2 standard. The V_{mp} is defined as the volume of material in the surface peaks at 10 % contact area. The V_{vv} represents the volume of the voids per unit area between 80 and 100 % of the surface material ratio curve. These parameters provide quantitative information of wear over time, the possible formation of wear debris during running-in and the volume of the deepest valley capable of holding such debris. The average volume V_{mp} and V_{vv} of the pristine samples before the test are 0.01 ± 0.04 $\mu m^3/\mu m^2$ and 0.04 ± 0.02 $\mu m^3/\mu m^2$, respectively. The effect of the abrasive particle size on the volume parameters is shown in **Fig. 10**. For both hard materials, an increasing SiC particle size from 22 µm to 200 µm increases the material removal (**Fig. 10a and c**). The peak and valley volume in the roughness profile is very shallow for a small SiC size but increases with SiC size, separating mild and severe wear damage. In contrast, Al_2O_3 abrasives exhibit a slighter variation in the peak and material valley volume due to the lower Al_2O_3 hardness.

The cross-section of the abraded surfaces against different SiC grit sizes is drawn schematically using R_v (maximum profile valley depth) and R_{sm} (mean width of the profile elements), as shown in **Fig. 11**. The grooves due to the 22 µm grit are shallow and homogeneously distributed with smooth edges, while the 200 µm abrasive particles induce deep and very wide grooves. Moreover, uneven grooves with many protrusions were also observed. The intermediate 82-125 µm grits generated mixed surface patterns, the grooves are uniform in most of the cases, but sometimes heterogeneous patterns are also observed.

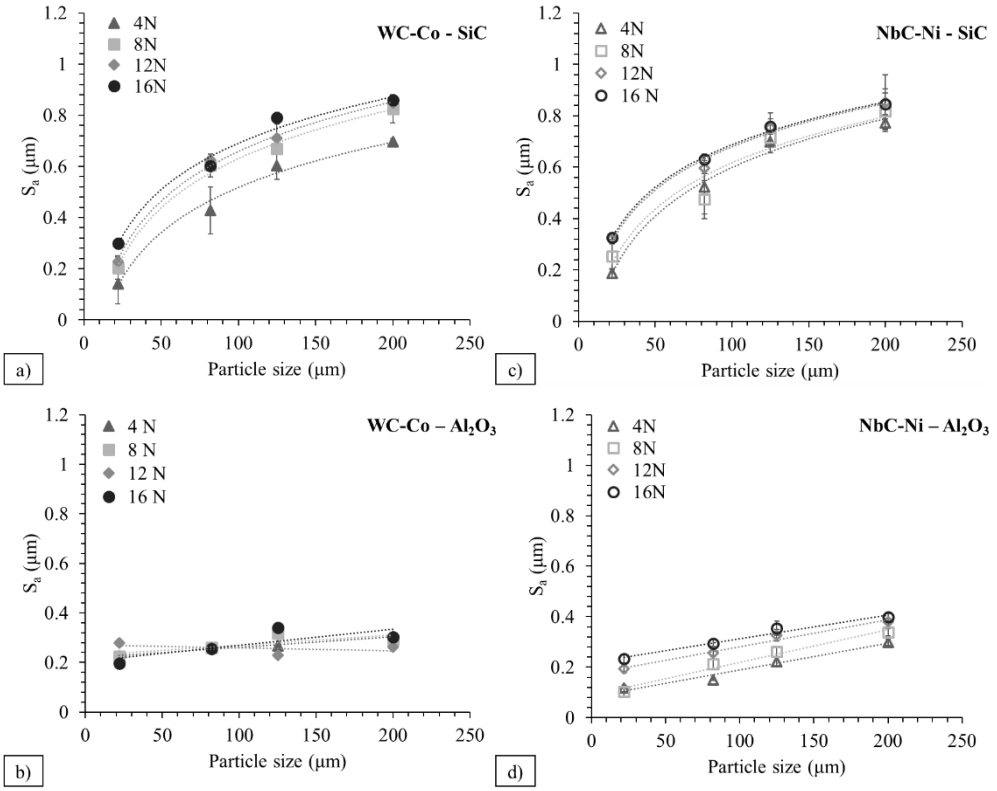

Fig. 9. Abrasive particle size vs 3D roughness of WC-Co against (a) SiC (b) Al_2O_3 and NbC-Ni cermet against (c) SiC (d) Al_2O_3 abrasives (Pristine S_a = 0.1 ± 0.02 µm).

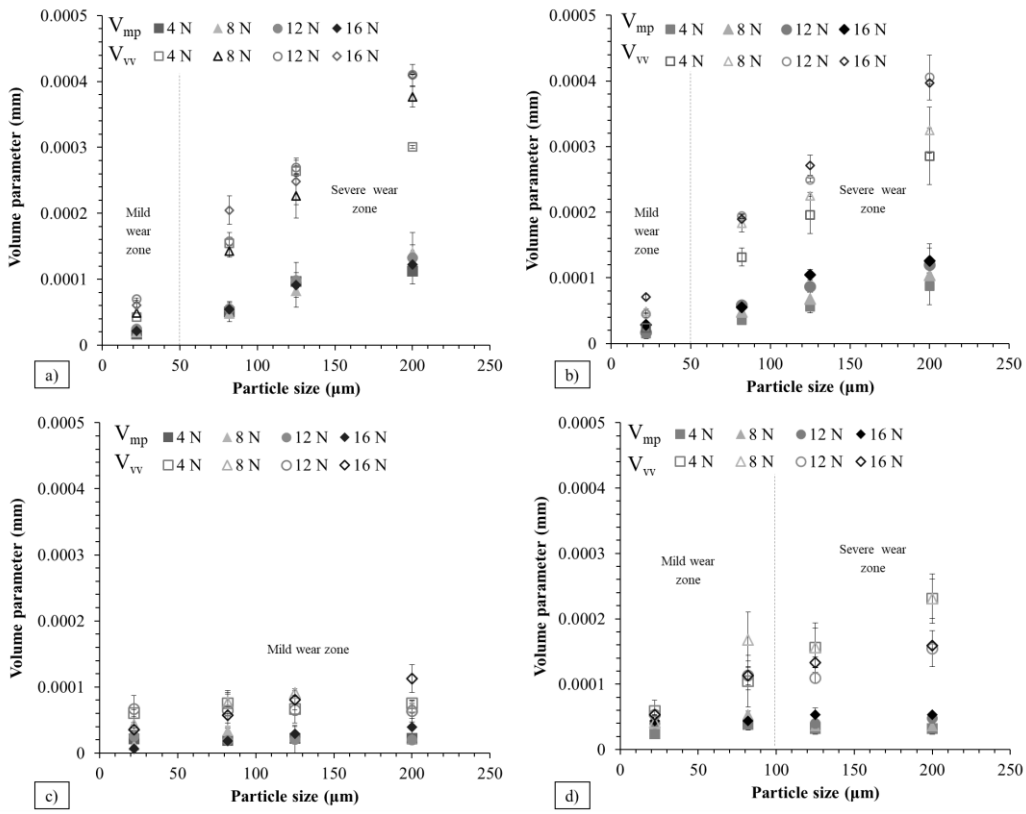

Fig. 10. Peak material (V_{mp}) and valley void volume (V_{vv}) of (a) WC-Co - SiC (b) WC-Co - Al_2O_3 and (c) NbC-Ni - SiC (d) NbC-Ni - Al_2O_3 cermet for different abrasive particle sizes.

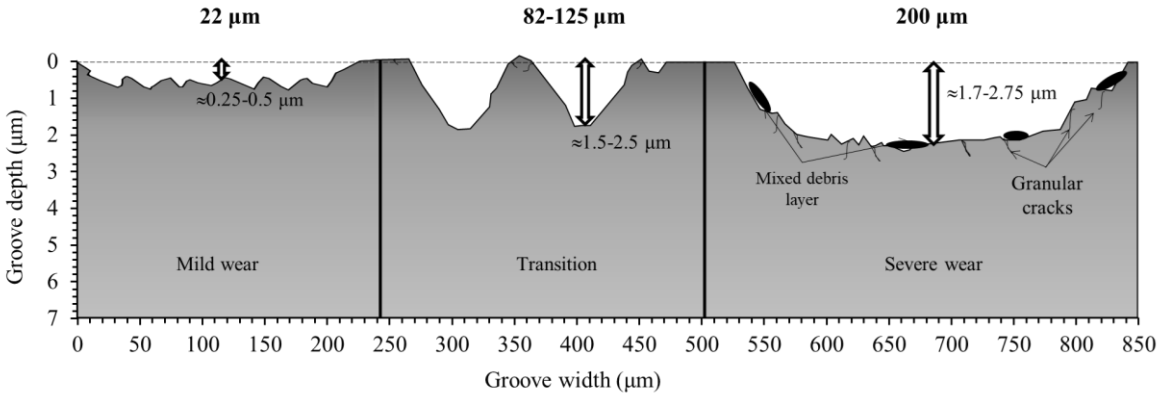

Fig. 11. Schematic cross-section of worn cermets surface as a function of SiC grit size.

3.4. Abrasive grit surface analysis

Fig. 12a-d shows SEM micrographs of SiC and Al_2O_3 counter surfaces after wear testing at different particle sizes. The pristine grit paper is shown in **Fig. 3**. The worn surface micrograph shows that different particle sizes experienced different damages. The coarse abrasive particles (200 µm) mainly experienced a fracture, attrition and shelling, whereas the finer abrasive particles (22 µm) are subjected to clogging and fragmentation. The attrition and fragmentation affect the shape and angularity of the abrasive particles. The transferred wear debris from the hard materials surface during abrasion covers/attaches to the tip of the abrasive particles (capping) changing the shape of the abrasive particles. The capping effect is mainly experienced with coarse particles. The clogging effect predominantly occurs with finer abrasives, which are covered with the build-up of wear residue that is extruded and pulled out from the surface of the hard material. **Table 5** highlights the quantitative data on material transfer of both cermets on the worn grit paper for both fine (22 µm) and coarse (200 µm) particles, as determined through EDS mapping. The results indicate that the transfer layer exhibits a mixed distribution of WC-Co on the grit surfaces, making it difficult to quantitatively determine the dominant phase removal (hard phase or binder) in response to fine and coarse abrasives. The presence of wear debris on the fine to coarse grit paper is confirmed by the concentrations of tungsten (W) and niobium (Nb) on the grit surface, although no clear trend is observed. In contrast, the Al_2O_3 grit shows minimal quantitative confirmation of transfer for tungsten (W), niobium (Nb), cobalt (Co) and nickel (Ni).

Apart from the microscopic observations, the abrasive grit surfaces before and after the wear test were further quantitatively analysed by optical profilometry (Keyence VR-5000) for both fine and coarse-grit papers. **Fig. 13** shows the result of S_z roughness (maximum profile height) of SiC and Al_2O_3 abrasive papers before and after wear testing against WC-Co at 16 N load. Test results indicate that the maximum profile height (S_z) of finer abrasives increased ≈1.2 and ≈2.6 times for SiC and Al_2O_3 abrasives (22 µm) after the wear test. The degree of material build-up due to WC-Co wear debris on the surface of Al_2O_3 abrasives is ≈2.2 times higher than for SiC abrasives. On the other hand, the S_z roughness of coarse SiC and Al_2O_3 abrasive paper is ≈1.5 and ≈1.2 times reduced after wear testing. The degree of particle damage for coarse abrasive particles shows an opposite trend, i.e. the SiC abrasives (≈1.2x) wear more than Al_2O_3 abrasives.

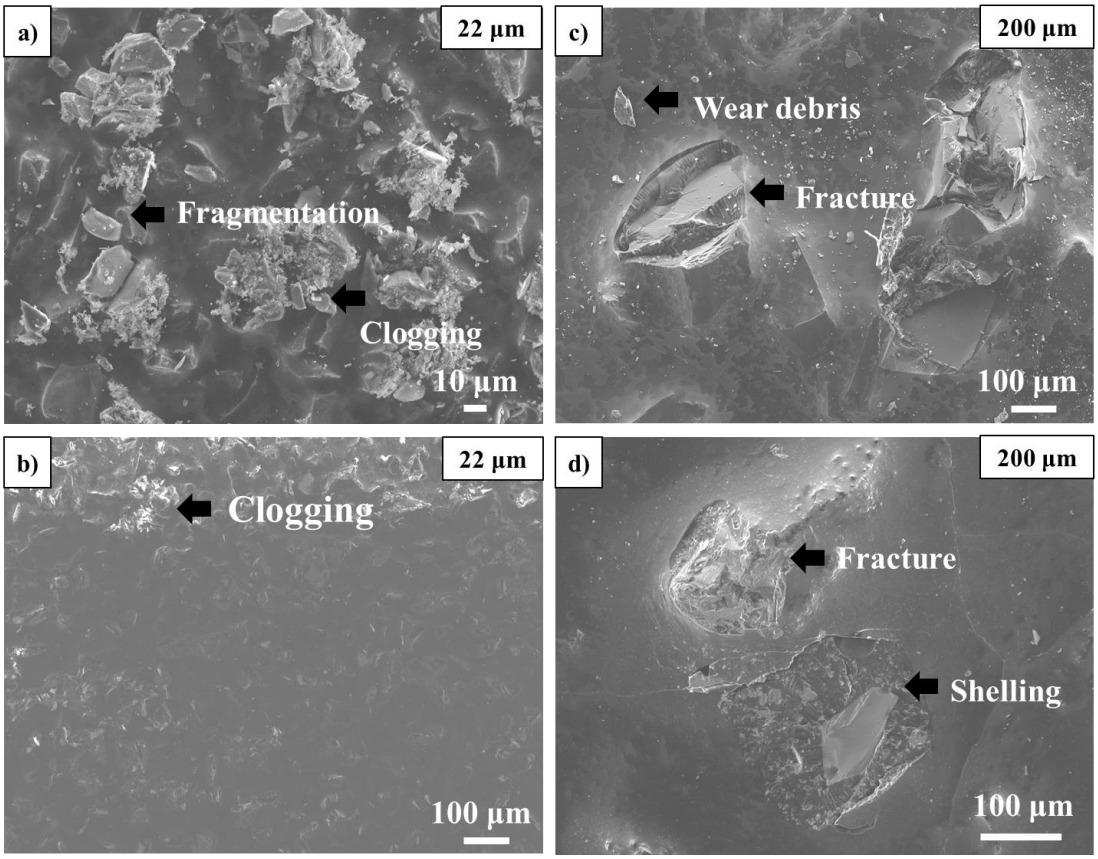

Fig. 12. SEM micrographs of (a and c) SiC and (b and d) Al_2O_3 grit papers after wear testing at 16 N load.

Table 5. EDS analysis of worn grit paper abraded against WC-Co (Magnification = x100, Working distance = 8 mm). Note: C and O values mentioned in the table are qualitative.

SiC grit paper							Al_2O_3 grit paper						
Particle size	22 µm			200 µm			Particle size	22 µm			200 µm		
Elements	Fresh	After		Fresh	After		Elements	Fresh	After		Fresh	After	
		WC	NbC		WC	NbC			WC	NbC		WC	NbC
C	72.2	70.9	71.6	70.7	72	70.8	C	57.9	60.7	58.2	69.4	71	69.1
Si	9.7	12.3	10.6	4.9	5.8	4.7	Al	5.7	1.2	2.5	0.6	0.8	2.6
O	17.9	15.3	15.8	24.1	20.8	23.6	O	35.3	36.8	37.8	28.1	26.5	24.6
W		1.2			1.2		W		0.2			0.1	
Co		0.1					Co		0.1				
Nb			1.6			0.5	Nb			0.2			0.3
Ni			0.3				Ni						
Mo						0.1	Mo						0.2
Na	0.2	0.2	0.1	0.3	0.2	0.3	Na	0.9	0.8	1.1	0.9	0.8	1
							Ca	0.2	0.2	0.2	1	0.8	2.2
Total (wt%)	100	100	100	100	100	100	Total (wt%)	100	100	100	100	100	100

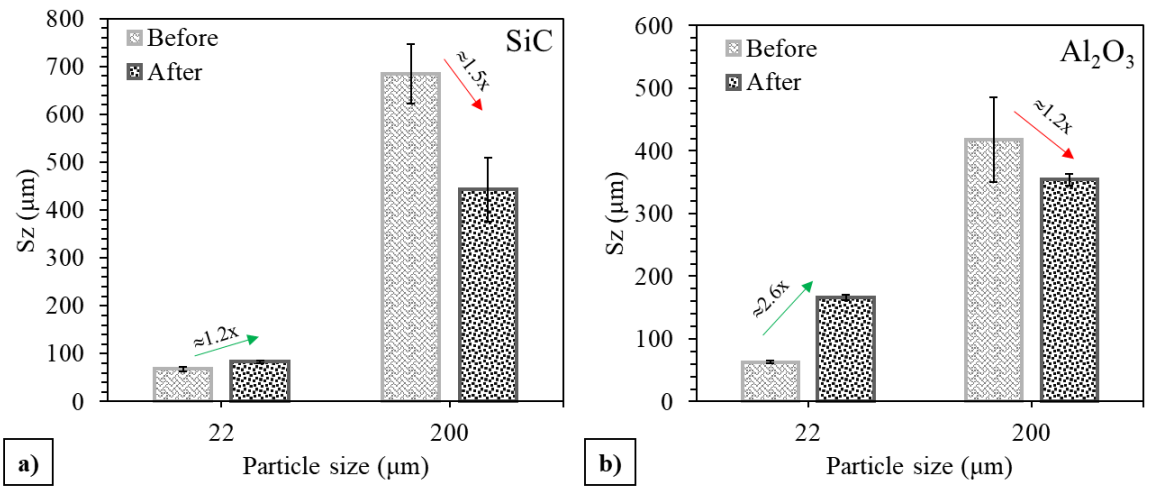

Fig. 13. S_z maximum profile height variation on fine and coarse abrasives before and after wear testing for (a) SiC and (b) Al_2O_3 paper.

4. Discussion

The relationship between abrasive particle size, hardness, wear rate and wear mechanism is complex and interdependent. The abrasive wear mechanism refers to the specific processes and interactions that occur when abrasive particles come into contact with a material surface, leading to material removal. When the abrasive particle size and hardness increase, the contact surface experiences more severe and localized stresses, leading to an increase in the abrasive wear rate. The change in wear rate is accompanied by prominent features of the abrasive wear micro-mechanism such as micro-cutting (metals) and fragmentation (ceramics). It is important to note that in some cases, the abrasive wear rate can also impact the overall wear mechanism. The wear rate determines the rate at which material is removed from the surface, which can subsequently affect other wear mechanisms such as surface fatigue and oxidation that come into play as the material is exposed to the environment. Therefore, while changes in wear mechanisms due to particle size and hardness are significant factors, the wear rate itself can also influence the overall wear mechanisms. In this discussion, the effect of changes in the abrasive wear rate with increasing load and abrasive particle characteristics such as hardness and size can be explained based on the material removal mechanism.

4.1. Hardness ratio effect

The tests against SiC abrasives consistently showed higher wear than for Al_2O_3 abrasives under equivalent conditions and significantly less scatter in wear and friction results. The material combinations can be ranked in order of increasing wear rate as: WC-Co against Al_2O_3 (**Fig. 5b**) < NbC-Ni cermet against Al_2O_3 (**Fig. 6b**) < WC-Co against SiC (**Fig. 5a)** < NbC-Ni cermet against SiC (**Fig. 6a**). This is in line with the experimental evidence of slip-line field theory on the contact between a discrete grit particle and a plane surface, predicting that the abrasive grit of any particle shape causes plastic scratching on inhomogeneous materials or cermets if the ratio of abrasive and surface hardness (H_a/H_s) is greater than 1.5 [30]. This implies that the abrasive grit should have a certain minimum hardness to scratch the material surface. In this case, the abrasive to sample surface hardness ratio for SiC is ≈2 and ≈1.4 for Al_2O_3 (**Table 1 and Table 4**). This hardness difference is also reflected in the current investigation, where the abrasive wear rate of both hard materials against SiC grit is an order of magnitude higher than with Al_2O_3. The aforementioned hardness ratio effect is further confirmed by the worn surface observations of hard materials, where the contact stress produced by Al_2O_3 abrasives is only able to deplete the binder in the hard materials surface at low load (4 N), as shown in **Fig. 7e and Fig. 8e**. On the other hand, SiC abrasives show plastic grooving with a mixture of carbide and binder phase removal at a low load (**Fig. 7a and Fig. 8a**). As the normal load applied on the abrasive particles is increased, the binder rich surface starts to deform plastically. The plastic flow or grooving will occur in the binder phase (Co, Ni) on the surface of the hard material when the contact pressure reaches a level of about three times the uniaxial yield stress. Plastic flow first occurs at the point where the yield criterion is first satisfied. On the other hand, the hard carbide phase starts fracturing once it exceeds the elastic limit. As soon as the contact pressure between the hard material and grit particle exceeds the compressive strength of the grit, the abrasive grits tend to deform, resulting in its fracture/fragmentation (**Fig. 12**) [35]. The subsequent material transfer was clear from the EDS results of the worn surfaces, where the Al and Si peaks were observed on the WC-Co and NbC-Ni surfaces (**Table 6**).

The self or re-sharpening effect of abrasives during the abrasive grinding process has been discussed in the literature [47]. The re-sharpening effect refers to the ability of abrasive particles to maintain sharp cutting edges during grinding processes, leading to improved material removal rates and grinding efficiency. SiC abrasives are known for their hardness and high friability, allowing them to retain their sharpness for extended periods, even under severe grinding conditions [48]. In contrast, Al_2O_3 particles have low friability than SiC, resulting in low affinity to self-sharpen [47, 48]. However, in the specific context of the pin abrasion study mentioned, the re-sharpening effect is assumed to be minimal. This

assumption is based on the observation that the present study follows a spiral trajectory where the pins come into contact with fresh abrasives each time. Since the pins are continuously in contact with fresh SiC or Al_2O_3 particles, the initial sharpness of the abrasives is less likely to degrade significantly. Consequently, the observed re-sharpening effect may not be a prominent factor in this particular scenario, as the fresh abrasives consistently provide effective cutting efficiency during each grinding cycle.

Table 6. EDS area analysis of WC-Co and NbC-Ni surfaces, worn under different loads and abrasive particle characteristics (measured surface area = 240 x180 μm^2, standard deviation (σ) = ± 0.7 wt%). Note: C and O data included in the table are only qualitative.

Material	Grit	Load (N)	Particle size (μm)	Surface composition (wt%)								
				W	Co	C	O	Nb	Ni	Mo	Si	Al
WC-Co	Pristine	-	-	85.4	8.7	5.9						
	SiC	4	22	83.8	5.4	8.9	1.9				0.1	
		16	200	77.1	8.1	11.8	2.2				0.8	
	Al_2O_3	4	22	77.3	6.9	9.9	5.1					0.9
		16	200	77.5	7.5	9.9	4.4					0.7
NbC-cermet	Pristine	-	-			14.0		63.7	13.0	9.3		
	SiC	4	22			16.2	2.4	61.9	9.8	9.3	0.4	
		16	200			18.1	3.5	56.4	12.2	9.3	0.5	
	Al_2O_3	4	22			17.2	4.8	59.8	9.0	8.7		0.4
		16	200			15.2	3.0	59.5	12.4	9.9		0.1

4.2. Particle size effect

The increase in the abrasive wear rate with increasing abrasive particle size can be explained by the grit/particle size effect. Literature indicates that the clogging and capping effects are contributors to the abrasive particle size effect. As experimentally verified by SEM micrographs of the grit papers (**Fig. 12**), the wear damage of grit particles can be attributed to capping (covering of the abrasives with wear debris), clogging (accumulation of debris particles formed between spaces of abrasive particles), fracture and fragmentation [33, 35]. However, the above effects are minimum contributors in this study as the test follows the spiral trajectory where the test pins are in contact with the fresh abrasives every time. As mentioned in the literature, several explanations have been found for the size effect observed in abrasive wear, where the wear rate remains independent of particle size after reaching the critical particle size (CPS). However, in most cases, the wear rate remains constant after the particle size of 100 μm (commonly referred to as CPS). As explained by Mishra and Finne [49], despite numerous previous explanations, the formation of a deformation-hardened surface layer or a thin surface debris layer in the near-surface region is the primary contributing factor to the size effect. This surface layer is commonly referred to as a mechanically mixed layer in the case of cermets, as clearly explained in [50]. In the present study, a similar surface effect was observed, where the fragmentation of abrasives produced wear debris that became embedded in the binder and formed a mechanically mixed surface layer as abrasive wear progressed. This phenomenon is clearly shown in Figs. 7c-d and 8c-d. The presence of this thin surface work-hardening layer near the surface increases the flow stress, leading to a reduced abrasive wear rate. However, this effect is more pronounced when abrasion occurs with coarse-grade abrasives, such as 125 and 200 μm particle sizes. This is observed beyond the critical particle size of

100 µm, as indicated in several literature and confirmed in the present study. These findings confirm that the mechanically mixed layer is more prominent when the abrasive grit size is large (coarse grit), while smaller particles (fine grit) predominantly contribute to binder phase removal and micro-cracking mechanisms.

Based on the wear test results, it can be observed that the load has minimal influence when using small abrasive grits (fine grits). However, an increase in particle size and load significantly contributes to changes in the abrasive wear rate for coarse abrasives. When the load is low (4 N) and the abrasive size is fine (22 µm), the main wear mechanisms involve binder extrusion and micro-fracture of carbide grains due to repeated contact fatigue (**Fig. 7 and Fig. 8**). When the load is increased to 16 N with the same abrasive grit, the wear rate slightly increased and dominant wear mechanism remains the same. This is because the higher packing density of finer grits indicates an increased number of particles in contact, which reduces the overall contact pressure as a result wear rate does not change significantly [51]. Conversely, with an intermediate particle size (82 µm), both NbC-Ni and WC-Co exhibit comparable abrasive wear rates as the load increases (**Fig. 5 and Fig. 6**). The observed wear mechanisms in this case are a combination of micro-fracture with micro grooving and material removal mechanisms (**Fig. 7 and Fig. 8**). For a grit particle size of 125 µm (medium grit), the dominant wear mechanism is grooving wear, followed by carbide cracking and fragmentation. However, the wear rate slightly decreases when the particle size changes from 82 µm to 125 µm. This effect is related to the specific cutting energy of the abrasive particles, which decreases as the particle reaches the critical depth of cut on the surface of the abrading materials, potentially leading to a transition in the wear mechanism. According to [49], the specific cutting energy decreased or remains steady as the particle size is increased above approximately 100 µm (critical depth of cut of 12 µm), which is considered the critical particle size (CPS). For a grit size of 200 µm, the wear mechanism remains the same, with extensive carbide cracking and fragmentation dominating the surface (**Fig. 5 and Fig. 6**). However, increasing the load results in an increased abrasive wear rate. It's worth noting that, besides the hard material test surface, the countersurface (grit paper) also experiences fracture damage, accompanied by attrition/fracture and shelling (**Fig. 12c and d**).

The volume parameters of the material ratio curve (**Appendix - III**) provide an estimate of the mild and severe wear transition of the hard materials (**Fig. 10**). For small grit sizes (22 µm), the ratio between the V_{mp} and V_{vv} indicates mild wear phenomena where the surface patterns are uniform and homogeneous (**Fig. 11**). However, the void volume increased significantly as the grit size increases (82 µm), resulting in a higher groove depth due to the removal of binder and carbide grains. Coarse abrasives (125-200 µm) exhibit high void volume, indicating severe wear with uneven and heterogeneous surface patterns. The S_a roughness displayed a logarithmic trend with increasing particle size (**Fig. 9a-b**). This trend can be attributed to the formation of a mechanically mixed surface layer (MML) or surface hardening layer near the cermets surface (**Fig. 7c-d and Fig. 8c-d**). The MML is formed due to the fragmentation of carbide grains and embedding, which increases flow stress and reduces the wear rate when in contact with coarse abrasive particles [50]. As a result, the surface roughness is decreased. In contrast, Al_2O_3 abrasives have a lower volumetric wear rate (V_{mp} and V_{vv}) on cermets, indicating mild wear phenomena. However, the roughness shows an increasing trend as the particle size increases. It is worth noting that the roughness of Al_2O_3 abrasives is significantly lower compared to SiC. There is no clear trend observed in roughness for WC-Co, with only a slight increment for NbC-Ni cermets against Al_2O_3 abrasives. This is likely due to the relatively low hardness ratio (≈1.4) between Al_2O_3 abrasives and cermets, which effectively prevents the cermets from penetration and grooving wear at low loads. The lower contact pressure generated by Al_2O_3 abrasives is apparently not sufficient enough to produce MML or surface hardening layer on the cermet surface. However, increased stress (load) leads to higher specific cutting energy on the abrasives, causing grain fragmentation and larger grooves on the cermets (as shown in

Fig. 7h), thereby increasing roughness. Additionally, due to this smaller hardness ratio, the increasing stress also causes fracture of the Al_2O_3 abrasive itself (**Fig. 12d)**.

4.3. Wear micro-mechanism comparison

Fig. 14 shows the worn surface comparison for WC-Co and NbC-Ni against small and large SiC particle sizes. The comparison shows that both hard materials have undergone different wear mechanisms. The WC-Co surface was exposed to partial removal of carbide grains due to carbide cracking and subsequent carbide pull-out against smaller abrasive particles, as shown in **Fig. 14a**. In contrast, NbC-Ni predominantly experienced binder depletion which undermines the NbC carbide grains. This effect exposes the worn surface by revealing the skeletal structure of the unsupported carbide grains (**Fig. 14c**). The remaining unsupported carbide grains were further wiped off as the sliding continues. The amount of binder removal from NbC-Ni cermet is comparatively higher than for WC-Co. To illustrate the abrasion mechanisms, **Fig. 15** provides schematics. In the case of WC-Co, the surface mainly experienced carbide fracture with transgranular cracks and grain pull-out. In contrast, NbC-Ni suffers from carbide pull-out as a result of binder depletion. It should be noted that in cermets, the wear of the binder plays a crucial role in maintaining the structural integrity of the composite. Specifically, the binder hardness is a determining factor in its durability. The enhanced wear-resistance of the binder matrix improves the protection of the carbide particles by slowing down the risk of discrete removal of material such as extrusion, pull-out or cracking. In this study, both cermets exhibited binder extrusion when the surface is abraded, however, the binder extrusion on the WC-Co surface was delayed compared to the NbC-Ni. This is attributed to the mechanical and chemical (interfacial) characteristics of the binder [52]. The micro-hardness of the Co binder is superior to that of the Ni binder. The higher stacking fault energy resulting in high deformation and moderate work hardening could be the possible reasons for the lower hardness of the Ni binder [34]. This effect increases the binder removal for NbC-Ni, resulting in a higher abrasive wear rate.

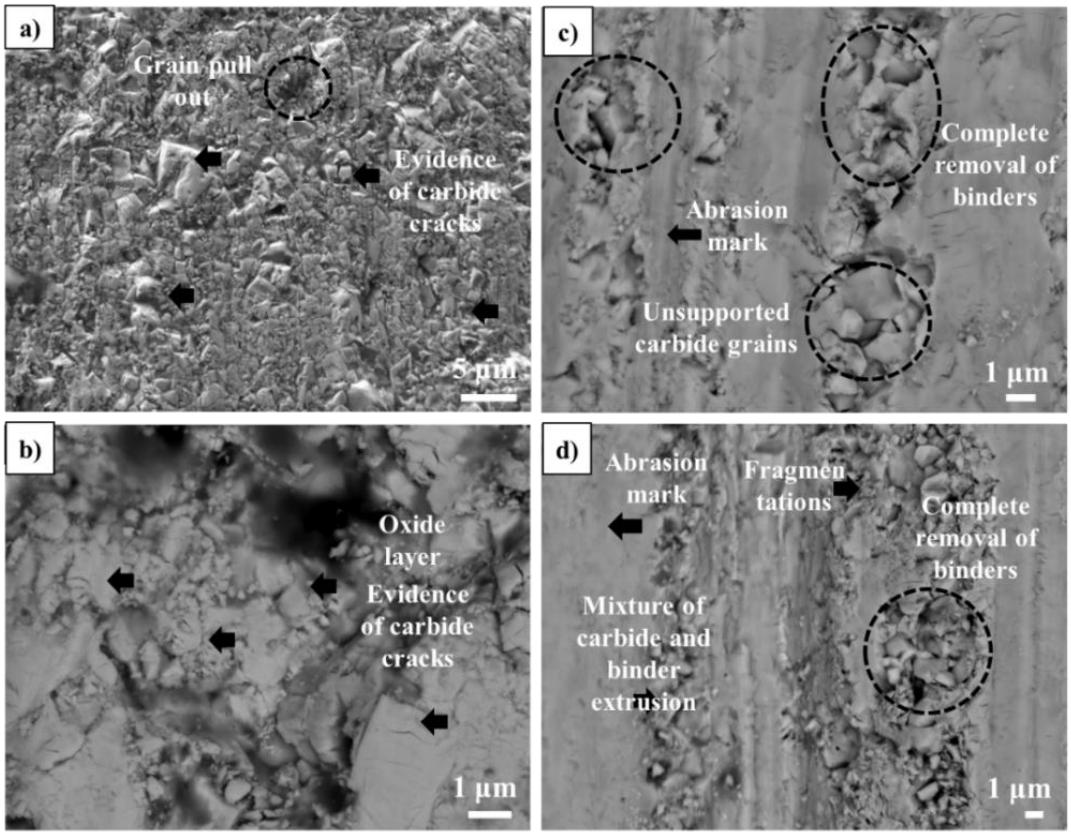

Fig. 14. Wear mechanisms comparison for (a) WC-Co against 22 µm, (b) WC-Co against 200 µm (c) NbC-Ni cermet against 22 µm and (d) NbC-Ni cermet against 200 µm SiC abrasive particles.

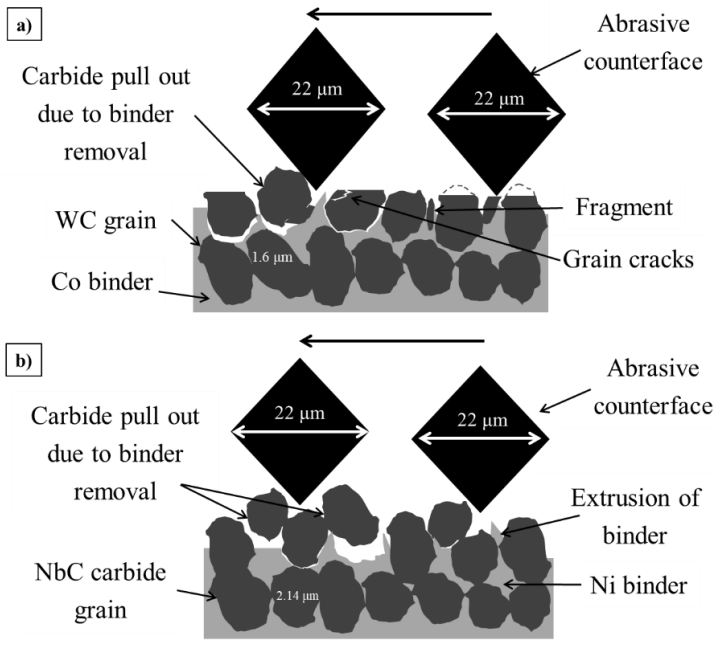

Fig. 15. Schematic wear mechanisms of (a) WC-Co and (b) NbC-Ni.

The presence of deep grooves and scratches on the samples indicates the abrasive action of highly loaded grit particles, leading to the removal of both the carbide and binder phases and significant fracture and fragmentation of WC/NbC carbide grains. However, it remains uncertain whether the removal of carbide and binder is a crucial precursor to carbide grain fracture [12]. Although some small fragments have been eliminated from the wear surface, others persist within the material structure, possibly due to their

re-embedment during continues sliding [12, 53]. Furthermore, SEM cross-section images (**Fig. 16**) provide evidence of both transgranular cracks extended approximately up to 10 µm beneath the surface of both NbC-Ni and WC-Co against SiC abrasives. NbC-Ni shows evidence of transgranular and intergranular cracks on the subsurface, whereas WC-Co shows only evidence of transgranular cracks. The intergranular cracks mainly occur in NbC-Ni due to the relatively lower wettability of NbC in the Ni matrix [34]. Besides the distribution of NbC in Ni is not homogeneous which generally creates Ni binder pools or lakes [54]. Therefore, the energy needed to break the bonding between NbC-Ni is comparatively lower than for WC-Co. On the other hand, the Al_2O_3 abrasives do not cause any subsurface damage on NbC-Ni and WC-Co due to their low abrasive hardness effect, as discussed earlier in this section.

Shipway [39] reported that the discrete removal of reinforced material can be delayed by using ductile reinforced materials and promoting strong adhesion between phases. In the present work, the adhesion between the NbC and Ni phases and the micro-hardness of the NbC-Ni composites is improved by Mo_2C alloying, as it provides solid solution strengthening [38]. However, the complete removal of binder induces a noticeable crater in NbC-Ni cermets in contrast to the WC-Co cermets during SiC abrasion. The formation of a crater confirms the significant removal or pull-out of carbide grains in NbC-based cermets, while WC-based cermets exhibit larger intragranular (transgranular) carbide cracks when abrading against hard abrasives. Therefore, the proposed compositions were not hard enough to hold the surface against abrasion as it has lower wettability and moderate interfacial strength between carbide and binder compared to WC-Co [10, 55]. This can be attributed to the absence of an interconnected structure between Ni in the NbC cermet, in contrast to the WC-Co composite, as reported in [10]. Thus, it can be concluded that the interfacial strength between the binder and carbide is an additional important phenomenon for having different wear-micro mechanisms. If the hardness and strength between the binder and carbides are weak, it is expected to dominate grain pull-out micro-mechanisms.

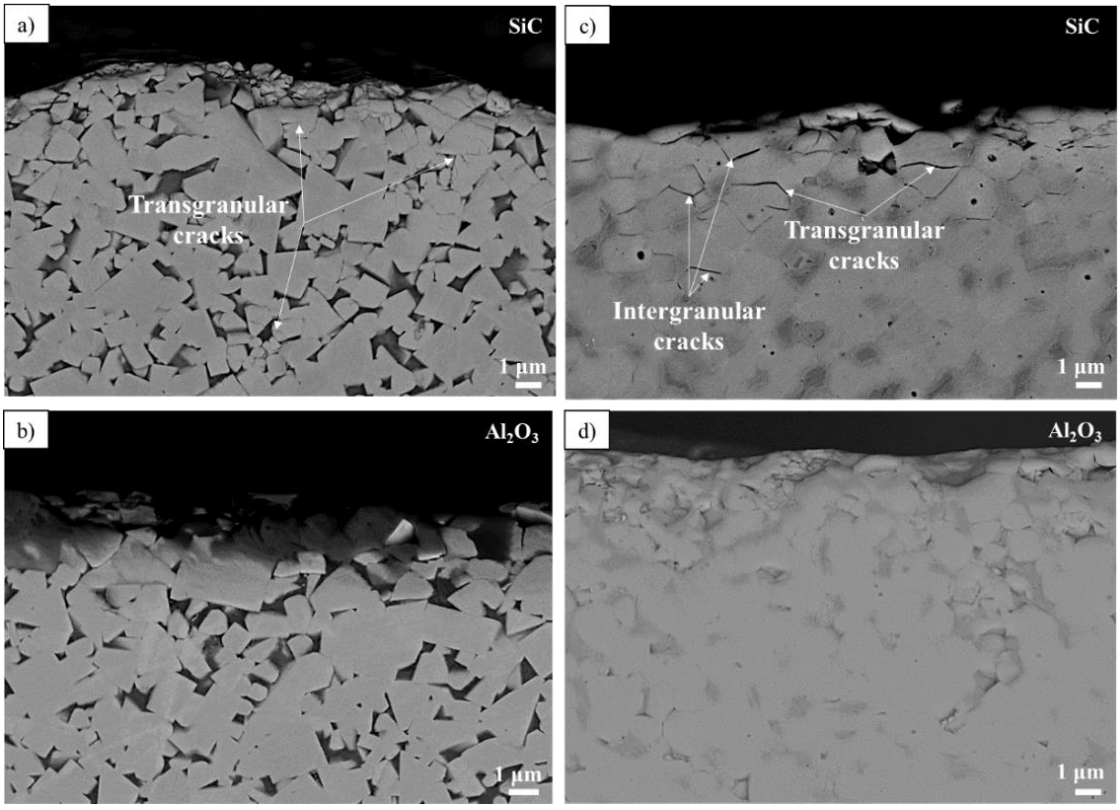

Fig. 16. Cross-section SEM of (a) WC-Co against SiC, (b) WC-Co against Al_2O_3 (c) NbC-Ni cermet against SiC and (d) NbC-Ni cermet against Al_2O_3 abrasive particles.

4.4. Wear debris analysis

The impact of wear debris on abrasive wear rates and wear mechanisms is influenced by several factors, including debris characteristics (such as size, shape, and hardness), surface properties of the contacting materials, applied load and specific wear conditions. During the pin abrasion test, where the specimen is continuously in contact with fresh abrasives, various phenomena indicate the influence of wear debris from abrasive grits on the wear rate and wear micro-mechanisms. One significant effect is that the generated wear debris acts as a third body within the contact region between the pin and abrasive grit surfaces [35, 56]. This presence of debris leads to the formation of surface micro-pits and alters the grooving trajectory, as evident from the worn surface morphology of the cermets (refer to **Fig. 17**). Furthermore, in some cases, the wear debris becomes embedded in the contacting surfaces, both in the pins and abrasive grits. This embedded debris act as inclusions, inducing local stresses that accelerate wear rates and cause changes in wear mechanisms [57]. However, there are also instances where the trapped wear debris on the cermets can serve as stress distributors between the contacting bodies. This stress distribution delays the wear of the contact bodies against each other, resulting in a reduced wear rate. However, it is important to note that the wear debris generated from the cermets surface can have negative effects on the abrasive grits, such as capping and clogging, which reduce cutting efficiency and contact pressure of abrasives [56]. In this particular case, these effects are minimized since the pins are always in contact with fresh abrasives. Moreover, fine wear debris formed as a mechanically mixed surface layer (MML) can act as a smooth hardening layer, increasing the flow stress and minimizing material removal [50]. Over time, the wear debris layer generally oxidizes when exposed to the surrounding air (tribo-oxidation), further contributing to a reduction in wear [57]. In conclusion, the presence of wear debris in the pin abrasion test can significantly affect wear rates and wear mechanisms. The specific influence of wear debris depends on its characteristics and interactions with the contacting surfaces, leading to either accelerated or reduced wear rates and changes in wear mechanisms.

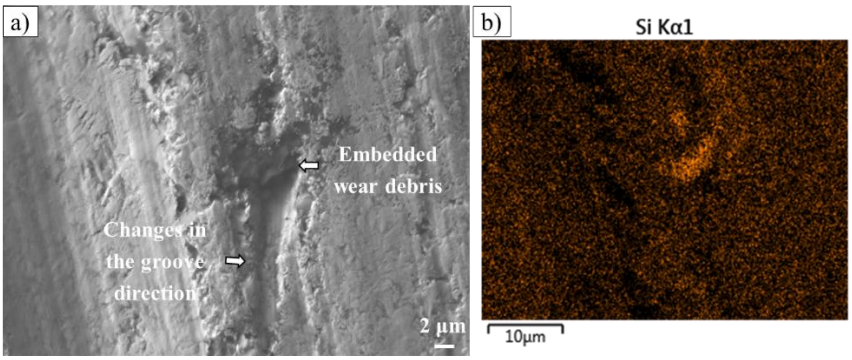

Fig. 17. (a) SEM micrographs of embedded SiC wear debris (b) EDS map confirms the presence of Si on the worn surface (Condition: WC-Co against SiC abrasive at 16 N load and 125 µm abrasive size).

4.5. Surface temperature and oxidation analysis

In addition to the mechanical wear, oxidation of wear debris also played a critical role in changing the friction and wear of hardmetals. During continuous sliding, some of the wear debris produced by fracture and fragmentation of carbide particles are getting wiped away, while some left on the wear surface experience oxidation due to frictional heating. It has been explained earlier [58, 59], that the fragmentation, oxidation, agglomeration and subsequent compaction of wear debris result in the formation of a tribo-oxidative layer in the wear track. The tribo-oxidation increases by increasing the sliding velocity and it subsequently reduces the abrasive wear rate and friction coefficient [58]. To assess the effect of abrasive particle size on frictional heating, the surface temperature was estimated theoretically according to equation (6) [59, 60],

$$\Delta T = \frac{\mu P v}{4a(K_a + K_s)} \quad (6)$$

$$\text{where, } a = \left(\frac{P}{\pi H_s}\right)^{0.5}$$

μ is the friction coefficient (see **Appendix - IV**), P is the system load (N), v is the sliding velocity (m/s), K_a and K_s are the thermal conductivity (W/m-K) of abrasives [**Table 4**] and surfaces [**Table 1**] and a is the contact radius of the real area of contact (m), H_s is the surface hardness (kg/mm^2) of the material.

The surface flash temperature is mainly influenced by the thermal properties of the contacting surfaces and the oxide film, the actual area of contact and heat loss caused by conduction and convection. The increase in surface flash temperature of both WC-Co and NbC-Ni cermet as the load and particle size is increased, as shown in **Fig. 18**. The higher surface temperature observed in the NbC-Ni cermet compared to the WC-Co cermet can be attributed to several factors related to the thermal properties of these materials and their respective counter-surfaces. These factors include the presence of oxide films and heat loss through conduction and convection mechanisms [59]. While the thermal conductivity of the Co (cobalt) binder is slightly lower than that of Ni (nickel) [61], the high thermal conductivity of WC enables the WC-Co cermet to efficiently dissipate heat and prevent excessive temperature build-up. In contrast, the NbC-Ni cermet exhibits lower thermal conductivity (see **Table 1**), resulting in less effective heat dissipation and higher surface temperatures. Further studies are required to clearly understand the primary reason for the surface temperature rise and its relationship to thermal properties. Additionally, the lower coefficient of thermal expansion of SiC (**Table 4**) results in a greater disparity in thermal expansion between the cermet and SiC, leading to uneven temperature distribution compared to Al_2O_3 abrasives. This non-uniform heating can cause localized high temperatures at the contact points between the abrasive particles and the cermet surface. As a consequence, such temperature spikes may lead to an increased flash temperature rise. To gain a comprehensive understanding of these effects and their implications, more research is needed in this direction.

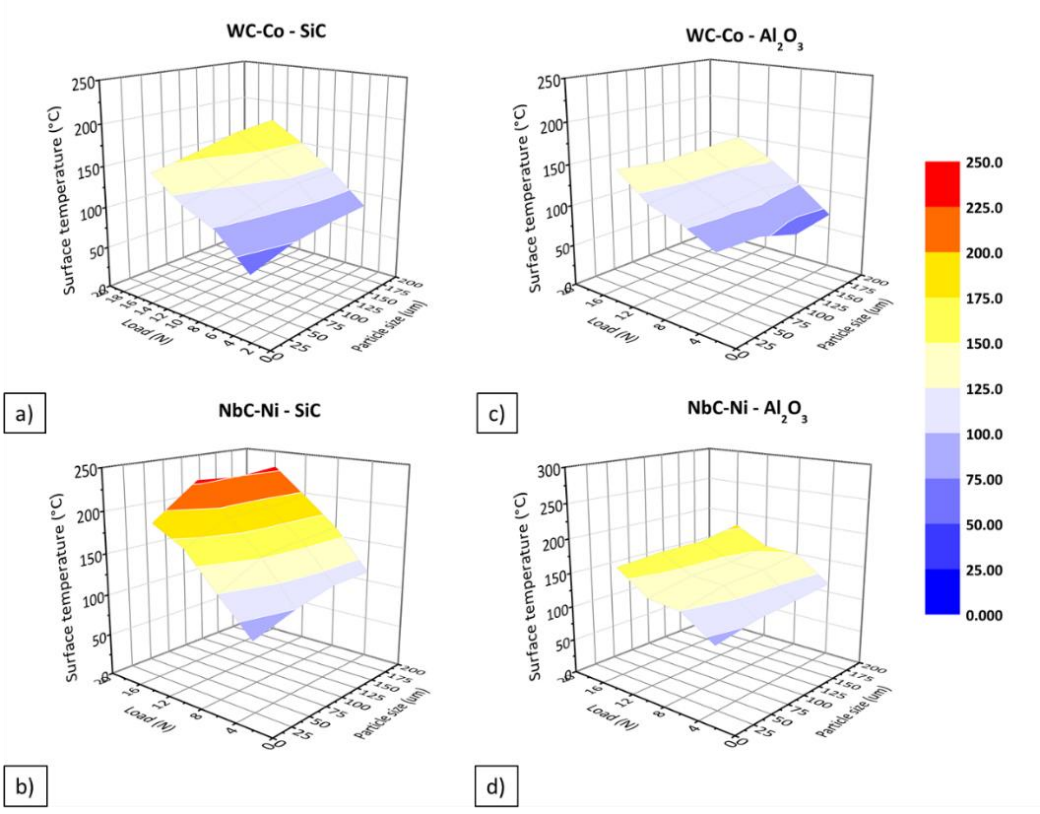

Fig. 18. A calculated surface temperature rise of WC-Co against (a) SiC and (c) Al_2O_3 abrasives and NbC against (b) SiC and (d) Al_2O_3 abrasives.

Furthermore, EDS spectra confirmed the presence of an oxide film on worn surfaces, as shown in **Table 5**. The results clearly show that the increase in load and particle size leads to a high surface temperature, which further results in an increase in the amount of oxygen on the wear track due to oxidation. The surface oxidation experienced on the worn surface for NbC-Ni cermet appears to be greater than the WC-Co, due to the higher surface temperature during frictional heating. Two potential factors contribute to oxidation during abrasion testing. The first factor is oxidation caused by the thermal effect, which occurs as a result of the increase in surface flash temperature due to friction between the cermet surface and abrasive grit particles [62]. The second factor is surface oxidation caused by the mechanical effect, which arises from surface damage and wear between the contacting bodies. This mechanical effect generates fragmented wear debris on the surface that rapidly oxidizes and forms a mild oxidative wear regime when exposed to the surrounding air [59, 63]. Both of these effects can occur simultaneously during abrasion, making it difficult to validate them solely through experimental studies. In our study, we aimed to theoretically calculate the surface flash temperature. Our calculations indicate that the surface temperature rises during abrasion, considering both the thermal and experimental factors of cermets and abrasives. Although the estimated surface temperature is comparatively lower than the required temperature for surface oxidation, the surface is covered with an oxidation layer that can be noticed from the experimental EDS mapping. Therefore, surface oxidation results from the combination of mechanical and thermal effects of wear debris.

It has been previously pointed out that covering worn surfaces with tribo-oxides plays a vital role in reducing the friction and abrasive wear rate of WC-12Co coating [59]. The formation of tribo-oxides in the wear track helps to reduce the real area of contact, concomitantly decreasing the friction coefficient [59]. The present study showed a similar oxidation effect on the wear track that is confirmed by backscatter electron images, as shown in **Fig. 14b**. The tribo-oxides appear larger on the worn surface only at a high load (16 N) and large abrasive particles (200 µm). This is probably because of the increased amount of wear debris due to grain fracture and fragmentation caused by the above condition, supported by the surface flash temperature rise. At a lower load (4 N) and fine particle size (22 µm), very mild oxidation prevails and the oxidative layer is relatively penetrable, which is further removed by plastic shearing. The tribo-oxidation formation in the wear track is dynamic, involving formation, removal and again reformation, referred to as 'oxidation-scrape-re-oxidation' [64]. For highly loaded (16 N) SiC abrasives with relatively larger particle sizes (200 µm), the oxide layer formation is interrupted by plastic indentation of abrasives and delaminating cracking of carbide grains, resulting in direct contact between the asperities.

4.6. Abrasive wear transition and severity of contact

It is evident that in brittle solids, the abrasive wear rate due to a fracture-dominated mechanism was almost an order of magnitude greater than the material removal by plastic deformation [65]. Possible factors such as the effect of abrasive particles (increasing the depth and sharpness of the indentation) and a decrease in the fracture toughness-to-hardness ratio of the hard material are likely to affect the wear transition mechanism from plastic deformation to fracture. Many researchers have proposed a concept for the wear transition of brittle materials from plastic deformation to fracture. Lawn *et al.* proposed that fracture mainly occurs when the indentation depth surpasses the critical indentation size and is proportional to the ratio ($H^2/\tau E$), where, H = hardness (HV), τ = fracture surface energy (N/m) and E = Young's modulus (GPa) of the material. Likewise, the ratio of (K_{1C}^2/H^3) is used in brittle materials to predict resistance to cracking as proposed in [66], where K_{1C} is the fracture toughness of the material. Hutchings applied the Lawn *et al.* concept for the transition of abrasive wear from plastic flow to Hertzian fracture of brittle surfaces by calculating the threshold particle size of the abrasive counterface. The threshold particle size (d_{TH}) was calculated according to the relation [66];

$$d_{TH} = \frac{K_{1Cs}^2 . E_s}{H_s^3} \quad (7)$$

Where K_{ICs}, E_s and H_s are fracture toughness, elastic modulus and hardness of the hard materials. The results are consistent with the current experimental evidence that fracture occurs earlier for NbC-Ni compared to WC-Co. The calculated threshold particle size for both WC-Co and NbC-Ni to initiate fracture-dominated failure is 26 µm and 13 µm, respectively. This research work only discusses the transition of cermets from ductile to brittle deformation and does not include the brittleness of abrasive particles. It is important to note that estimating the brittleness of abrasive particles is a complex task that involves considering multiple factors. These factors include particle characteristics, intrinsic K_{1C} values, the presence of internal defects and the adhesive resins used in sand particle abrasion. Considering all these factors is essential for accurately estimating the brittleness of abrasive particles and optimizing their performance in various applications.

The severity of contact (SoC) has been developed by many researchers to predict the particle motion and transition from mild to severe wear mode of ceramics [67-69]. The SoC during abrasive wear is influenced by load, abrasive particle characteristics (size, shape and hardness) and material properties (hardness and fracture toughness). Thakare *et al.* [68] compared the effect of changes in particle size on abrasive wear rate using the modified SoC as proposed by Adachi *et al.* [69]. The author additionally includes the brittleness factor to check the wear mode transition from ductile to brittle. Similarly, Vashishtha *et al.* have revised the severity of contact for a pin abrasion tester by incorporating additional parameters such as the ratio of the size of the abrasive particles to the carbide grain size and hardness, the fracture toughness of the abrasives and surface [59]. However, they did not take into account the shape factor or circularity of abrasive particles that affect the severity of contact during abrasive wear. The circularity or roundness factor of abrasives is considered a crucial factor that directly impacts the cutting efficiency and severity of abrasive particles [35]. However, it is essential to recognize that abrasion removal mechanisms depend on multiple factors, including the material and abrasive properties, contact conditions, and wear rate, rather than solely relying on particle circularity. Factors such as system load and the spacing ratio between indentation forces and frictional forces can influence surface damage due to circularity [70]. Reports suggest that sharp abrasive particles cause abrasive damage through indentation wear, rather than grooving wear [71]. Our previous study [55] found that cermets did not exhibit significant changes in the abrasion rate as the roundness factor increased. However, it is observed that rounded or near-spherical abrasives exhibited grooving wear, leading to increased binder removal and pull-out, while angular abrasives broke and embedded into the surface of the cermets. In this study, we assume a direct proportionality between circularity and abrasive wear due to the material removal caused by grooving wear. By incorporating the roundness factor with other wear parameters, we can achieve a more precise quantification of the severity of wear caused by abrasion, considering the shape characteristics of the abrasive particles and their influence on the material removal process. Hence, this paper modified the relationship of contact severity expressed in Vashishtha *et al.* by additionally incorporating the circularity index (F_a) [70]. Therefore, the severity of contact for the pin on abrasive grit paper is expressed as;

$$SoC = \left(\frac{P}{A_{ws}}\right)\left(\frac{H_a}{H_s}\right)\left(\frac{K_{1Ca}}{K_{1Cs}}\right)\left(\frac{D_a}{D_s}\right)(F_a) \quad (8)$$

where P is the applied load (N), A_{ws} is the wear scar area (mm), H_a and H_s are the abrasive and surface hardness (kg/mm^2), K_{1Ca} and K_{1Cs} are the fracture toughness of abrasives and surfaces (MPa.m$^{1/2}$), D_a and D_s are the abrasive particle and carbide grain sizes (µm) and F_a is the circularity of the abrasives [**Table 3**].

The calculated SoC for WC-Co and NbC-Ni cermet was plotted against the specific wear rate (SWR) in **Fig. 19**. The specific wear rate increases with an increase in the severity of contact. The severity of

contact does not only change the abrasive wear rate but also affects the observed mechanism. However, the results show that the overall wear rates and the mechanisms obtained are likely to be controlled by the microstructural characteristics of the material to fracture of WC and NbC grains under increased indentation loading. Moreover, the severity of contact is also influenced by the hardness of the abrasives used. As observed, the SoC of NbC-Ni cermet and WC-Co showed a lower value when tested against Al_2O_3 than SiC abrasives. Despite the equal testing conditions, WC-Co with a relatively higher fracture toughness showed lower specific wear rates than the NbC-Ni cermet. In **Fig. 19**, the horizontal dashed lines indicate the transition from plastic grooving to fracture for NbC-Ni and WC-Co, where the fracture occurs earlier for NbC-Ni than for WC-Co. The change in failure of WC-Co by plastic grooving to fracture occurs due to a decrease in fracture toughness [59]. Moreover, the abrasive wear produced by Al_2O_3 abrasives for both NbC-Ni (●) and WC-Co (▲) shows that the observed wear rate within the plastic deformation limit is substantially lower compared to the SiC abrasives, as shown in **Fig. 19**. This result further confirmed the effect of the abrasive hardness on the abrasive wear rate and wear mechanism of cemented carbides and ceramics. For SiC abrasives, a particle size below 82 µm resulted in strongly dominated plastic grooving wear, but this changed to fracture-dominated failure when the particle size increased. The abrasive wear mechanisms corresponding to the predominated failure mode, as observed from worn surface examination, are shown in the diagram using vertical dotted lines. Zone I indicates a failure mode dominated by ductile mechanism, where the surfaces experienced plastic deformation, extrusion/removal of binder due to plastic grooving and micro-fracture. The surfaces experienced a brittle mechanism such as extensive cracking, fracture and grain fragmentation dominated failure in Zone III. In the transition area, marked as Zone II, the surfaces showed both micro-grooving and fracture failure modes.

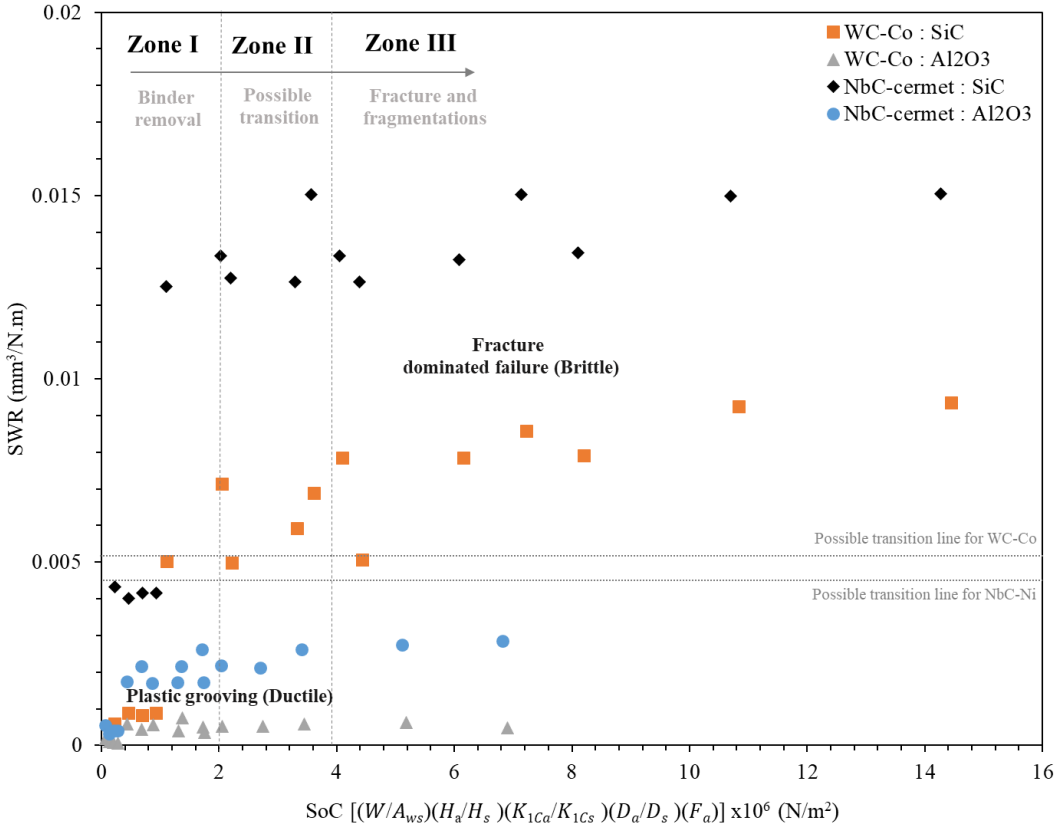

Fig. 19. The specific wear rate of NbC-Ni and WC-Co vs. severity contact.

Conclusions

The closed two-body abrasion behaviour of WC-Co and NbC-Ni hard materials against SiC and Al_2O_3 abrasives at different loads (4-16 N) and abrasive particle sizes (22-200 µm) was assessed. The test results highlight the following:

- Multiphase materials, such as WC-Co and NbC-Ni cermets, showed an elevated abrasive wear rate with an increase in both the size and hardness of abrasive particles. This increase was attributed to a transition in wear mechanisms, shifting from plastic grooving to fracture and fragmentation.
- The comparison showed that NbC-Ni has a 37-86 % and 66-83 % higher abrasive wear rate than WC-Co for SiC and Al_2O_3 grit, respectively, irrespective of the comparable material micro-hardness. This is due to the good wettability of tungsten carbide in cobalt, a homogeneous WC distribution, high plastic deformation energy of the Co binder and fracture toughness of WC-Co, which are all relatively higher than for the NbC-Ni cermet.
- For both NbC-Ni and WC-Co, the abrasive wear rate increased with increasing load and abrasive particle size, however, the increase was more pronounced with the abrasive particle size than the load.
- The abrasive wear rate initially increased when the abrasive particle size increased from 22 µm to 82 µm, gradually increased between 82-125 µm and became independent at higher grit size, demonstrating the abrasive particle size effect.
- Changing from SiC to Al_2O_3 abrasives reduced the abrasive wear rate by an order of magnitude for both NbC-Ni and WC-Co, indicating the abrasive hardness effect.
- The effect of tribo-oxidation in the wear track during abrasive wear increased with a rise in surface temperature.
- The changes in wear mechanism due to the abrasive particle size have been attributed to an increase in the severity of contact accompanied by an increased load per particle. The specific wear rate was correlated with the severity of contact for both NbC-Ni and WC-Co materials, clearly indicating a wear mode transition from plastic deformation to fracture.

Literature shows the potential of NbC-Ni cermets against crater wear compared to WC-Co cemented carbides in cutting tool applications. The current research confirms this potential of NbC-Ni cermet against flank wear in two-body abrasive wear conditions. On the other hand, it lacks both material (wettability) and mechanical (fracture toughness and flexural strength) properties to achieve an abrasion resistance comparable to the WC-Co cemented carbide reference material. In the future, the fracture toughness of NbC-Ni cermet should be improved with alternative grain growth inhibitors and binder contents and subsequently compared to the abrasion resistance of WC-Co.

Acknowledgement

(1) The authors are gratefully acknowledge the funding for Scientific Research Flanders (FWO, Flanders) in the context of the project. G.0772.16N.
(2) To our professor and colleagues at the Soete Laboratory, prof. dr. ir. Dieter Fauconnier, ir. Ruben Saverwyns, dr. ir. Wouter Ost, ir. Jonathan Vancoillie, Michele De Waele, and dr. ir. Vitaliy Bliznuk for providing the technical support.

References

[1] Mari D. Cermets and Hardmetals. Reference Module in Materials Science and Materials Engineering: Elsevier; 2016.

[2] Spriggs GE. A history of fine grained hardmetal. Int J Refract Met Hard Mater. 1995;13:241-55.

[3] Moulin JJ, Wild P, Romazini S, Lasfargues G, Peltier A, Bozec C, et al. Lung Cancer Risk in Hard-Metal Workers. Am J Epidemiol. 1998;148:241-8.

[4] Tang L, Wang P, Graedel TE, Pauliuk S, Xiang K, Ren Y, et al. Refining the understanding of China's tungsten dominance with dynamic material cycle analysis. Resources, Conservation and Recycling. 2020;158:104829.

[5] Woydt M, Huang S, Vleugels J, Mohrbacher H, Cannizza E. Potentials of niobium carbide (NbC) as cutting tools and for wear protection. Int J Refract Met Hard Mater. 2018;72:380-7.

[6] Huang S, Liu R, Li L, Van der Biest O, Vleugels J. NbC as grain growth inhibitor and carbide in WC–Co hardmetals. Int J Refract Met Hard Mater. 2008;26:389-95.

[7] Woydt M, Mohrbacher H. The use of niobium carbide (NbC) as cutting tools and for wear resistant tribosystems. Int J Refract Met Hard Mater. 2015;49:212-8.

[8] Huang SG, Nie HB, Guo XY, Vleugels J, Huang JH, Mohrbacher H, et al. Microstructural investigation and machining performance of NbC-Ti(C0.5N0.5) matrix cermets. Int J Refract Met Hard Mater. 2019;84:105038.

[9] Huang SG, Liu C, Liu BL, Vleugels J, Huang JH, Lauwers B, et al. Microstructure and mechanical properties of (Nb,W,Ti)(C,N)-Ni solid solution cermets with 6 to 20 wt% Ni. Int J Refract Met Hard Mater. 2022;103.

[10] Huang JH, Huang SG, Zhou P, Lauwers B, Qian J, Vleugels J. Microstructure and mechanical properties of WC or Mo2C modified NbC-Ni cermets. Int J Refract Met Hard Mater. 2021;95:105440.

[11] Hu J, Chou YK. Characterizations of cutting tool flank wear-land contact. Wear. 2007;263:1454-8.

[12] Gant A, Gee MJIJoRM, Materials H. Abrasion of tungsten carbide hardmetals using hard counterfaces. 2006;24:189-98.

[13] Jiménez AE, Bermúdez MD. 2 - Friction and wear. In: Davim JP, editor. Tribology for Engineers: Woodhead Publishing; 2011. p. 33-63.

[14] Larsen-Basse J. Abrasive wear of some titanium-carbonitride-based cermets. Materials Science and Engineering: A. 1988;105-106:395-400.

[15] Kübarsepp J, Klaasen H, Pirso JJW. Behaviour of TiC-base cermets in different wear conditions. 2001;249:229-34.

[16] Choi Y, Baik NI, Lee JS, Hong SI, Hahn YD. Corrosion and wear properties of TiC/Ni–Mo composites produced by direct consolidation during a self-propagating high-temperature reaction. Composites Science and Technology. 2001;61:981-6.

[17] Klaasen H, Kübarsepp JJW. Abrasive wear performance of carbide composites. 2006;261:520-6.

[18] Qi X, Eigen N, Aust E, Gärtner F, Klassen T, Bormann R. Two-body abrasive wear of nano- and microcrystalline TiC–Ni-based thermal spray coatings. Surf Coat Technol. 2006;200:5037-47.

[19] Juhani K, Pirso J, Viljus M, Letunovits S. Two-body dry abrasive wear of Cr3C2-Ni cermets. Proc Estonian Acad Sci Eng. 2006;12:368-76.

[20] Klaasen H, Kollo L, Kübarsepp J. Mechanical properties and wear performance of compression sintered TiC based cermets. Powder Metall. 2007;50:132-6.

[21] Hussainova I, Pirso J, Antonov M, Juhani K, Letunovitš S. Erosion and abrasion of chromium carbide based cermets produced by different methods. Wear. 2007;263:905-11.

[22] Figiel P, Zimowski S, Klimczyk P, Dziwisz T, Jaworska L. Mechanical and tribological properties of TiC-based composites for ED machining. Archives of Materials Science and Engineering. 2008;33:83-8.

[23] Pirso J, Viljus M, Juhani K, Letunovitš S. Two-body dry abrasive wear of cermets. Wear. 2009;266:21-9.

[24] Antonov M, Hussainova IJTI. Cermets surface transformation under erosive and abrasive wear. 2010;43:1566-75.

[25] Pirso J, Viljus M, Letunovitš S, Juhani K, Joost RJW. Three-body abrasive wear of cermets. 2011;271:2868-78.

[26] Ren X, Peng Z, Hu Y, Wang C, Fu Z, Yue W, et al. Abrasive wear behavior of TiCN cermets under water-based slurries with different abrasives. Tribology International. 2013;66:35-43.

[27] Kübarsepp J, Pirso J, Juhani K, Viljus M. Developments in cermet design, technology and performance. International Journal of Materials and Product Technology. 2014;49:160-79.

[28] Iparraguirre I, Lozada L, Ibarreta F, Martinez R, Sanchez J. Liquid phase sintering of (Ti, W) C-Ni-Co-Cr cermets: Microstructure and abrasive wear behavior. Solid State Phenomena: Trans Tech Publ; 2018. p. 1-8.

[29] Woydt M, Huang S, Cannizza E, Vleugels J, Mohrbacher H. Niobium carbide for machining and wear protection–Evolution of properties. Metal Powder Report. 2019;74:82-9.

[30] Zum Gahr K-H. Microstructure and wear of materials: Elsevier; 1987.

[31] Krakhmalev PV. Abrasion of ultrafine WC-Co by fine abrasive particles. Transactions of Nonferrous Metals Society of China. 2007;17:1287-93.

[32] Krakhmalev PV, Sukumaran J, Gåård A. Effect of microstructure on edge wear mechanisms in WC–Co. Int J Refract Met Hard Mater. 2007;25:171-8.

[33] Sahariah BJ, Vashishtha N, Sapate SJMRE. Effect of abrasive particle size on friction and wear behaviour of HVOF sprayed WC-10Co-4Cr coating. 2018;5:066424.

[34] García J, Ciprés VC, Blomqvist A, Kaplan BJIJoRM, Materials H. Cemented carbide microstructures: a review. 2018.

[35] Hutchings I, Shipway P. 6 - Wear by hard particles. In: Hutchings I, Shipway P, editors. Tribology (Second Edition): Butterworth-Heinemann; 2017. p. 165-236.

[36] Coronado J, Sinatora AJW. Effect of abrasive size on wear of metallic materials and its relationship with microchips morphology and wear micromechanisms: Part 1. 2011;271:1794-803.

[37] Krakhmalev PJTL. On the abrasion of ultrafine WC–Co hardmetals by small SiC abrasive. 2008;30:35-9.

[38] Huang SG, Vleugels J, Mohrbacher H, Woydt M. Microstructure and tribological performance of NbC-Ni cermets modified by VC and Mo2C. Int J Refract Met Hard Mater. 2017;66:188-97.

[39] Shipway PH, Hogg JJ. Dependence of microscale abrasion mechanisms of WC-Co hardmetals on abrasive type. Wear. 2005;259:44-51.

[40] Shetty DK, Wright IG, Mincer PN, Clauer AH. Indentation fracture of WC-Co cermets. Journal of Materials Science. 1985;20:1873-82.

[41] Pierson HO. Handbook of Refractory Carbides and Nitrides: Properties, Characteristics, Processing and Applications: Elsevier Science; 1996.

[42] Thiele S, Sempf K, Jaenicke-Roessler K, Berger L-M, Spatzier J. Thermophysical and Microstructural Studies on Thermally Sprayed Tungsten Carbide-Cobalt Coatings. J Therm Spray Technol. 2011;20:358-65.

[43] Hamblin MG, Stachowiak GW. A multi-scale measure of particle abrasivity. Wear. 1995;185:225-33.

[44] Basu B, Kalin M. Tribology of ceramics and composites: a materials science perspective: John Wiley & Sons; 2011.

[45] Wang AG, Hutchings IM. The number of particle contacts in two-body abrasive wear of metals by coated abrasive papers. Wear. 1989;129:23-35.

[46] Sukumaran J, Kalácska Á, Neis PD, Fauconnier D, De Baets P. From single asperity to real scale in the wear of agricultural tine. Wear. 2019;426-427:14-26.

[47] Mohan R, Deivanathan R. A review of self-sharpening mechanisms of fixed abrasive tools. International Journal of Mechanical Engineering and Technology. 2019;10.

[48] Marinescu ID, Rowe WB, Dimitrov B, Inasaki I. 11 - Abrasives and Abrasive Tools. In: Marinescu ID, Rowe WB, Dimitrov B, Inasaki I, editors. Tribology of Abrasive Machining Processes. Norwich, NY: William Andrew Publishing; 2004. p. 369-455.

[49] Misra A, Finnie I. On the size effect in abrasive and erosive wear. Wear. 1981;65:359-73.

[50] Antonov M, Hussainova I, Pirso J, Volobueva O. Assessment of mechanically mixed layer developed during high temperature erosion of cermets. Wear. 2007;263:878-86.

[51] Gåhlin R, Jacobson S. The particle size effect in abrasion studied by controlled abrasive surfaces. Wear. 1999;224:118-25.

[52] Penrice TW. Alternative binders for hard metals. Journal of Materials Shaping Technology. 1987;5:35-9.

[53] Larsen-Basse J, Perrott CM, Robinson PM. Abrasive wear of tungsten carbide—cobalt composites. I. Rotary drilling tests. Materials Science and Engineering. 1974;13:83-91.

[54] Genga RM, Rokebrand P, Cornish LA, Nelwalani N, Brandt G, Kelling N, et al. High-temperature sliding wear, elastic modulus and transverse rupture strength of Ni bonded NbC and WC cermets. Int J Refract Met Hard Mater. 2020;87:105143.

[55] Rajendhran N, Pondicherry K, Huang S, Vleugels J, De Baets P. Influence of abrasive characteristics on the wear micro-mechanisms of NbC and WC cermets during three-body abrasion. Wear. 2023:205007.

[56] Coronado J, Sinatora AJW. Effect of abrasive size on wear of metallic materials and its relationship with microchips morphology and wear micromechanisms: Part 2. 2011;271:1804-12.

[57] E8 - Mechanisms of wear. In: Neale MJ, editor. Tribology Handbook (Second Edition). Oxford: Butterworth-Heinemann; 1995. p. E8.1-E8.3.

[58] Vashishtha N, Sapate S. Effect of Experimental Parameters on Wear Response of Thermally Sprayed Carbide Based Coatings %J Materials Research. 2019;22.

[59] Vashishtha N, Sapate SG. Abrasive wear maps for High Velocity Oxy Fuel (HVOF) sprayed WC-12Co and Cr3C2−25NiCr coatings. Tribology International. 2017;114:290-305.

[60] Liu Y, Erdemir A, Meletis EI. A study of the wear mechanism of diamond-like carbon films. Surf Coat Technol. 1996;82:48-56.

[61] Woydt M, Mohrbacher H, Vleugels J, Huang S. Niobium carbide for wear protection – tailoring its properties by processing and stoichiometry. Metal Powder Report. 2016;71:265-72.

[62] Quinn TFJ. Review of oxidational wear: Part I: The origins of oxidational wear. Tribology International. 1983;16:257-71.

[63] Stachowiak G, Batchelor AW. Engineering tribology: Butterworth-Heinemann; 2013.

[64] Hutchings I, Shipway P. Tribology: friction and wear of engineering materials: Butterworth-Heinemann; 2017.

[65] Moore MA, King FS. Abrasive wear of brittle solids. Wear. 1980;60:123-40.

[66] Hutchings IM. Ductile-brittle transitions and wear maps for the erosion and abrasion of brittle materials. J Phys D: Appl Phys. 1992;25:A212-A21.

[67] Hsu SM, Shen M. Wear prediction of ceramics. Wear. 2004;256:867-78.

[68] Thakare M, Wharton J, Wood R, Menger CJW. Effect of abrasive particle size and the influence of microstructure on the wear mechanisms in wear-resistant materials. 2012;276:16-28.

[69] Adachi K, Hutchings IM. Wear-mode mapping for the micro-scale abrasion test. Wear. 2003;255:23-9.

[70] Fang L, Zhao J, Li B, Sun K. Movement patterns of ellipsoidal particle in abrasive flow machining. J Mater Process Technol. 2009;209:6048-56.

[71] Ordoñez MFC, Amorim CLG, Krindges I, Aguzzoli C, Baumvol IJR, Figueroa CA, et al. Microstructure and micro-abrasive wear of sintered yttria-containing 316L stainless steel treated by plasma nitriding. Surf Coat Technol. 2019;374:700-12.

Appendix – I

Different abrasive wear testing and property comparison maps for cermets and cemented carbide											
Reference	**Cermets**	**Binder content**	**Mechanical Properties**			**Test method / standard**	**Abrasive**		**Test conditions**	**Findings**	**Observed wear micro-mechanisms**	**Missing link**
			HV	**F.T**	**B.S**		**type**	**size**				
Abrasive wear of some titanium-carbonitride-based cermets [14]	Ti(C,N)-Ni-Mo-WC (d= 1 -4)	12.5 wt% Ni - 11 wt% Mo - 10 wt% WC	1500-1800	7-11	-	Modified ASTM B611, (block-on-wheel)	SiO_2, SiC and diamond	SiO_2 = 100 µm SiC = 81.5 µm Diamond = 1 µm	L = 10.9 N , 5 N (SiC, SiO_2)	1. The hardness effect of different abrasive countersurface explained 2. Wear mechanisms of TiCN cermets produced from SiC and diamond abrasives are similar 3. SiO_2 abrasives cause shallow grooves on the surface of the cermet and no relative changes are noticed	• Plastic indentation and micro-spall formation for SiC and diamond abrasives • Fine scale micro-spall formation for SiO_2 (quarts) abrasives	An explanation for the abrasive grit size, critical particle size and their effect of wear micro-mechanisms transition has not been explained
Behaviour of TiC-based cermets in different wear conditions [15]	TiC-NiMo (d_{TiC}=1.9-2.2)	20–50 NiMo (Ni:Mo 4:1, 2:1)	890-1430	-	1090-1680	Modified ASTM B611, (block-on-wheel)	SiO_2	0.1-0.3 mm	SD = 100 m	1. Cermets with FeNi composition with relative hardness compete with WC-Co 2. Differences in wear behaviour of hardmetals and cermets may be related to their structural components	-	No clear explanation for the effect of abrasive properties and their wear mechanisms response is unknown
	TiC-FeNi (d_{TiC}=1.9-2.2)	20–40 FeNi (5, 8, 14, 17 Ni in binder)	1000-1520	-	1380-2450							
	WC-Co (d_{WC}=1-2.2)	Co (10-2 0 wt%)	1030-1500	-	1900-3000							

Corrosion and wear properties of TiC-Ni–Mo composites produced by direct consolidation during a self-propagating high-temperature reaction [16]	TiC_x-Ni-Mo (x = 0.84, 0.87)	Ni, Mo (Ni = 49.5 wt%, Mo = 0 - 8.5 wt%)	-	-	-	Modified ASTM G132	Conditions not specified	Conditions not specified	Conditions not specified	1. Mo increase decreases the wear rate of TiC-Ni cermet due to the increased interfacial bonding strength	-	An explanation for the effect of abrasive properties and their wear mechanisms response are unknown
Abrasive wear performance of carbide composites [17]	TiC-NiMo	Ni:Mo (2:1, 4:1) (20-50 wt%)	1000-1400	-	1700-2200	Modified ASTM B611, (block-on-wheel	SiO_2	0.1-0.2 mm	L = 3 N, V=0.24 m/s, SD = 140 m	1. Wear resistance: WC-Co > TiC-FeNi > TiC-NiMo 2. An increase in modulus of elasticity decreases the abrasive volume loss 3. Flexural strength shows a nonlinear trend in abrasive wear 4. The performance of carbide composites in abrasive is controlled by the stiffness of the alloy	Material removal mechanisms: binder extrusion → transgranular cracking of the carbides	No clear explanation for the effect of abrasive properties and their wear mechanisms response is unknown
	TiC-FeNi	FeNi (20-40 wt%)	1050-1450	-	1500-2400							
	WC-Co	Co (10-20 wt%)	1000-1350	-	2300-3100							
Two-body abrasive wear of nano- and microcrystalline TiC–Ni-based thermal spray coatings [18]	(Ti,Mo)(C,N) – NiCo (coating)	NiCo (25 Ni-20 Co vol%)	870-940	-	-	Pin on drum (JIS H8615)	SiC	30-200 µm	L = 30 N, SD = 30 mm, V = 3 mm/min	1. Nanocrystalline coating provides better performance than microcrystalline for all the particle sizes 2. Critical particle size lies between 45 µm to 100 µm	• Nanocrystalline coating: cutting and ploughing • Microcrystalline coating: Transition from binder removal to hard phase fracture and fragmentations	No explanation of the abrasive grit size effect on the wear micro-mechanisms of cermets
Two body dry abrasive wear of TiC–NiMo	TiC-NiMo	Ni:Mo (1:1, 2:1, 4:1)	810-1650		730-2450	Modified block-on-ring	Alumina grinding wheel (HV = 1940)	0.25 mm	L = 10, 20 N, V = 2.8 m/s, SD = 100 m	1. Wear volume loss ∝ applied Load and sliding distance up to 100 m 2. Increasing the binder decreases the bulk	• Plastic deformation • Subsurface cracks • Binder phase extrusion and	No explanation of the abrasive grit size effect of abrasives on

Cermets [19]		(20-60 wt%)								hardness of the system which increases the volume loss	removal followed by the fracture	the wear micro-mechanisms
Mechanical properties and wear performance of compression sintered TiC based cermets [20]	TiC-FeNi (d_{TiC} = 2-2.2)	FeNi (20-40 wt%)	HRA 88.7-91.3	-	1400-2300	Modified block-on-ring (ASTM G65-94)	SiO_2	0.1-0.2 mm	L = 3 N, V = 0.24 m/s, SD = 145 m	1. No abrasion effect on ordinary vacuum sintering and sinter/hipping (gas compression during sintering) 2. Sinter/hipping increases the rupture strength of TiC cermets which perform better adhesive wear resistance	-	No explanation for wear mechanisms, abrasive grit size, shape and hardness effect
Erosion and abrasion of chromium carbide based cermets produced by different methods [21]	Cr_3C_2-Ni	10–30 Ni	LPS: 920–1420	9.5–18.0	-	Modified block-on-ring (ASTM B611)	Alumina grinding wheel (HV = 1900)	0.25 mm	L = 20 N, V = 2.8 m/s, SD = 50 m	1. Lower binder fraction (10 wt% of Ni) shows better performance than high binder fraction in Cr_3C_2 carbides 2. Reactive sintering grades outperform conventional sintering grades 3. Similar abrasion mechanisms were observed for both fabrication techniques but reactive sintering has some advantages due to strong interfacial bonding and homogenous distribution	• An increase (↑) in the binder wt% produces deeper grooves on the cermet surface, carbide fracture and intergranular cracks	No clear explanation of the abrasive size, shape and harness effect
			Reactive sintering: 890–1450	9.8–18.5	-							
Mechanical and tribological properties of TiC–based composites for ED machining [22]	TiC-Ni-Mo	10–30 vol% (Ni, Mo) (Ni:Mo = 3:2)	1405–1664	7.8–9.5	-	Pin on disc abrasion tester (DIN 50330)	SiC Grit paper	80 µm	L = 29.4 N, SD = 20.6 m, V = 600 rpm	1. An increase in hardness decreases the abrasive wear	-	No clear explanation for the effect of abrasive properties and their wear mechanisms

												response is unknown
Two-body dry abrasive wear of cermets [23]	TiC-Ni-Mo	NiMo (20–60 wt%) (Ni:Mo = 4:1, 2:1, 1:1)	810–1650	-	730–2450	Block on ring test (ASTM B611-85)	Alumina grinding wheel (HV = 1940)	0.3 mm	L = 20 N, V = 2.8 m/s, SD = 100 m	1. Wear volume loss of the cermets saturated approximately 100 m sliding distance 2. Wear volume showed a similar trend for Cr_3C_2 and WC-Co 3. Cermets with a lower binder ratio (wt%) provide better performance than a higher binder ratio	• TiC-20 wt% Ni: Formation of grooves and crater and no evidence of binder removal • TiC-20 wt% Ni: Deep grooves and ridges, binder extrusion, no direct determination of fracture and fragmentation	No explanation for the abrasive grit size and hardness effect
	Cr_3C_2-Ni	10–30 Ni	780–1330	-	670–910						• Cr_3C_2–10 wt% Ni: Plastic deformation of carbides and binder matrix, micro-pits appeared due to the fracture and pull-out of carbide grains • Cr_3C_2–30 wt% Ni: Deep grooves and ridges, material pileup due to the plastic deformation, formation of parallel and median cracks	
	WC-Co	6–20 Co	880–1380	-	1370–2500						• WC–6 wt% Co: Plastic deformation and binder extrusion followed by carbide pull out • WC–20 wt% Co: Deep grooves due to severe plastic deformation, fragmentation noticed	

Cermets surface transformation under erosive and abrasive wear [24]	TiC-NiMo (d = 2-4 µm)	NiMo (12 vol%)	-	-	-	Modified block on steel wheel (ASTM G65-94)	SiO_2 HV=1078	0.2-0.3 mm	L = 130, 195, 490 N V = 2.39 m/s SD = 718 m	1. Wear resistance: Cr_3C_2-Ni > WC-Co > TiC-NiMo 2. An explanation for the mechanically mixed layer formation is found	• Formation of the mechanically mixed layer due to the re-embedment of carbide and sand fragments on the binder matrix • Formation of subsurface transgranular and intergranular cracks just below the mechanically mixed layer	No explanation of the abrasive grit size effect and hardness effect
	Cr_3C_2-Ni (d = 2-4 µm)	Ni (12 and 33 vol%)	-	-	-							
	WC-Co (d = 2-4 µm)	Co (12 vol%)	-	-	-							
Three-body abrasive wear of cermets [25]	TiC-NiMo	20–60 wt% (Ni:Mo 4:1, 2:1, 1:1)	810-1650	10.4-22.9	-	Modified block-on-ring (ASTM B611)	SiO_2	0.1-0.3 mm	L = 40 and 400 N, V = 2.2 m/s, SD = 100 m	1. The hardness ratio between cermets and abrasives explained based on a different hardness range 2. No linear dependency between the wear coefficient and applied load (as predicted by Archard's equation) 3. Despite the similar hardness and binder ratio, the wear rate is noticed different	• Plastic deformation as the dominant wear mechanism and small carbide fracture was noticed when the hardness of the abrasives was harder than cermets • At high loads, severe plastic deformation is followed by the carbide fracture if the cermet is harder than the surface. Material removal due to binder extrusion at low load • Plastic deformation and fracture of carbide occur simultaneously if the hardness of abrasives and cermet is equal	No further explanation of the abrasive grit size effect
	Cr_3C_2-Ni	10–30 wt% Ni	780-1330	7.9-14.5	-							
	WC-Co	6-20 wt% Co	890-1580	14.7-37.3	-							

Abrasive wear behavior of TiCN cermets under water-based slurries with different abrasives [26]	Commercial TiCN cermet (d_{TiC} = 0.5-2)		2200	-	-	Modified Wet sand rubber wheel test (ASTM G105)	SiC (HV=2900-3000), Al_2O_3 (HV=2000-2100), SiO_2 (HV=1000-1100)	SiC (0.45 mm), Al_2O_3 (0.6 mm), SiO_2 (0.58 mm)	L = 225 N, V = 498 RPM, SD = 60 Km, slurry concentration = 5 – 40 wt%	1. Abrasive volume fraction of cermets against abrasive slurry : SiC > Al_2O_3 > SiO_2 abrasives based on the hardness ratio between abrasive and cermets 2. Wear rate increased with the increase in abrasive mass fraction	• SiC abrasives: plastic deformation and micro-grooving, fracture associated with carbide pull-out (micro-pits) • Al_2O_3 abrasives: plastic deformation of binder phase (binder removal) • SiO_2 abrasives: plastic deformation (binder removal)	No further explanation of the abrasive grit size and shape effect
Developments in cermet design, technology and performance [27]	TiC-NiMo (d_{TiC} = 2)	Ni:Mo (1:1,2:1, 4:1) (20-60 wt%)	750-1700	-	700-2550	Modified block-on-steel wheel (ASTM B611)	SiO_2	0.1-0.3 mm	L = 40 and 200 N, V = 2.2 m/s, SD = 50 m	1. Wear coefficient : Cr_3C_2-Ni > TiC-NiMo (4:1) > TiC-NiMo (2:1) > TiC-FeNi > TiC-FeNi (1:1) 2. H_a/H_m > 1.2 : plastic deformation and fracture H_a/H_m < 0.9	• TiC- NiMo cermets : Plastic deformation (50-60 wt%) • Cr_3C_2-Ni cermet: mixed plastic deformation and fracture • Hardness ratio > 1.2: plastic deformation and fracture • Hardness ratio < 0.9: microcracks and falling out • Hardness ratio = 0.9-1.2: binder squeeze out and removal	No further explanation of the abrasive grit size effect
	TiC-FeNi	FeNi (20-40 wt%)	1250-1390	-	1800-2500							
	Cr_3C_2-Ni (d_{Cr3c2}) = 4-6)	10–30 wt% Ni	700-1400	-	580-1400							
Liquid phase sintering of (Ti,W)C-Ni-Co-Cr cermets: Microstructure and abrasive wear behavior [28]	(Ti,W)C-Ni-Co-Cr	18.5–26.6 vol% (Ni, Co, Cr)	950–1300	-	-	Pin on disc abrasion tester (ASTM G132)	SiC Grit paper	180 µm	L = 4.7 N, V = 150 rpm, SD = 1200 m	1. An increase in the binder phase increases the wear	-	No explanation for wear mechanisms, abrasive grit size effect and hardness effect

Niobium carbide for machining and wear protection – Evolution of properties [29]	NbC-Ni, Co, NiVC, NiMo, NiMoVC, $NiMo_2CVC$	Co (12 vol%) Ni (6-12 vol%)	1197-1499	5.78-10.3	626-1599	Dry sand rubber wheel (ASTM G65)	SiO_2	265 µm	L = 130 N, SD = 6000 m, V= .04 m/s	1. NbC offers improved wear resistance than cemented carbides under dry abrasive wear condition 2. Dry abrasive wear independent from micro-hardness	-	No specific wear mechanism and particle size effect explained
Two-body abrasive wear of cemented carbide (Abrasive grit size and hardness effect)												
Grooving Wear [30]	WC-Co (dWC= 1.35 µm)	Co (6-25 vol%)	950-1400	-	-	Pin on abrasive paper test	SiC, Al2O3 and flint	63 µm and 145 µm	L = 1.4, 2.8, 4.9 MPa	1. Abrasive particle hardness resulting in different micro-wear mechanisms 2. Fine-grained WC outperforms coarse-grade WC against micro-cracking 3. WC-Co with high carbide: fine grade outperforms coarse 4. WC-Co with high cobalt: coarse grade outperforms fine grade	• SiC abrasives: grooving and micro-cracking (leads to flaking) • Al2O3 abrasives: plastic deformation and WC/WC or WC/Co interface fracture • Flint abrasives: plastic deformation (Co binder removal)	No further explanation of the abrasive particle size effect and their wear mechanism explanations
Abrasion of ultrafine WC-Co by fine abrasive particles [31]	WC-Co (dWC= 0.3-4.5 µm)	Co (5-14 wt%)	1050-2150	5.6-24	3180-5100	Pin on Disc and edge on disc test (ASTM G132)	SiC	21.8 µm and 125 µm	SD = 27 m, V = 0.5 m/min, L = 2 N	1. Pin on disc: Finer SiC abrasives the coarse grade WC-Co outperforms submicron grade WC-Co 2. Edge on disc: Coarse grade WC-Co has a 25-40% higher wear rate than fine grade WC-Co 3. The ratio between carbide size and abrasive particle size effect is explained	• Ultrafine grade WC-Co: micro-ploughing • Coarse grade WC-Co: transition from grain pull-out to binder removal followed by WC detachment • Fine abrasives against WC-Co: binder removal and pull of WC grains • Coarse abrasives against WC-Co:	No further explanation for critical particle size and size effect for a range of grit sizes

											plastic deformation, fracture and fragmentation, pull-out	
Effect of microstructure on edge wear mechanisms in WC–Co [32]	WC-Co (dWC= 0.3-4.9 µm	Co (3-11 wt%)	1150-1950	7-19	2100-4700	Edge on disc	SiC	5 µm (fine) and 200 µm (coarse)	L= 2 N, 15 N, V=0.5, 1 cm/s, SD = 30 m		• Fine abrasives: binder removal and pull of WC grains • Coarse abrasives: Flaking to ploughing transition	No further explanation for critical particle size and particle size effect with different size ranges
Effect of abrasive particle size on friction and wear behaviour of HVOF sprayed WC-10Co-4Cr coating [33]	WC-Co-Cr coating (d = 1.5 µm)	Co (10 vol%) Cr (4 vol%)	1138-1158	4.4-5.8	-	Pin abrasion test	SiC	36 – 150 µm	L = 30, 60 N, V = 0.25, 1 m/s, SD = 1256 m	1. Critical particle size: 100 µm 2. An increase in the particle size increases the wear up to 2.5-4 times for 30 N and 1.5-1.6 times higher for 60 N	• The particle size effect showed a transition in wear mechanisms from fatigue and plastic formation to fracture failure along with the load	Particle size effect clarified for WC-Co-Cr coatings

Appendix – II

Number of particles in contact and the herz contact pressure.

Particle size (µm)	Particles in nominal contact area (N)	Particles in real contact area (n)	CP for single abrasive particle (GPa)		Nominal contact pressure (GPa)		CP for the real area of contact (GPa)	
			WC	NbC	WC	NbC	WC	NbC
22	48811.52	476.60	16.35	16.99	0.45	0.46	2.09	2.18
82	3513.50	23.66	10.09	10.49	0.66	0.69	3.52	3.65
125	1511.99	9.06	8.65	8.99	0.75	0.78	4.15	4.31
200	590.62	3.00	7.28	7.56	0.87	0.90	5.04	5.24

Appendix - III

Surface material ratio curve:

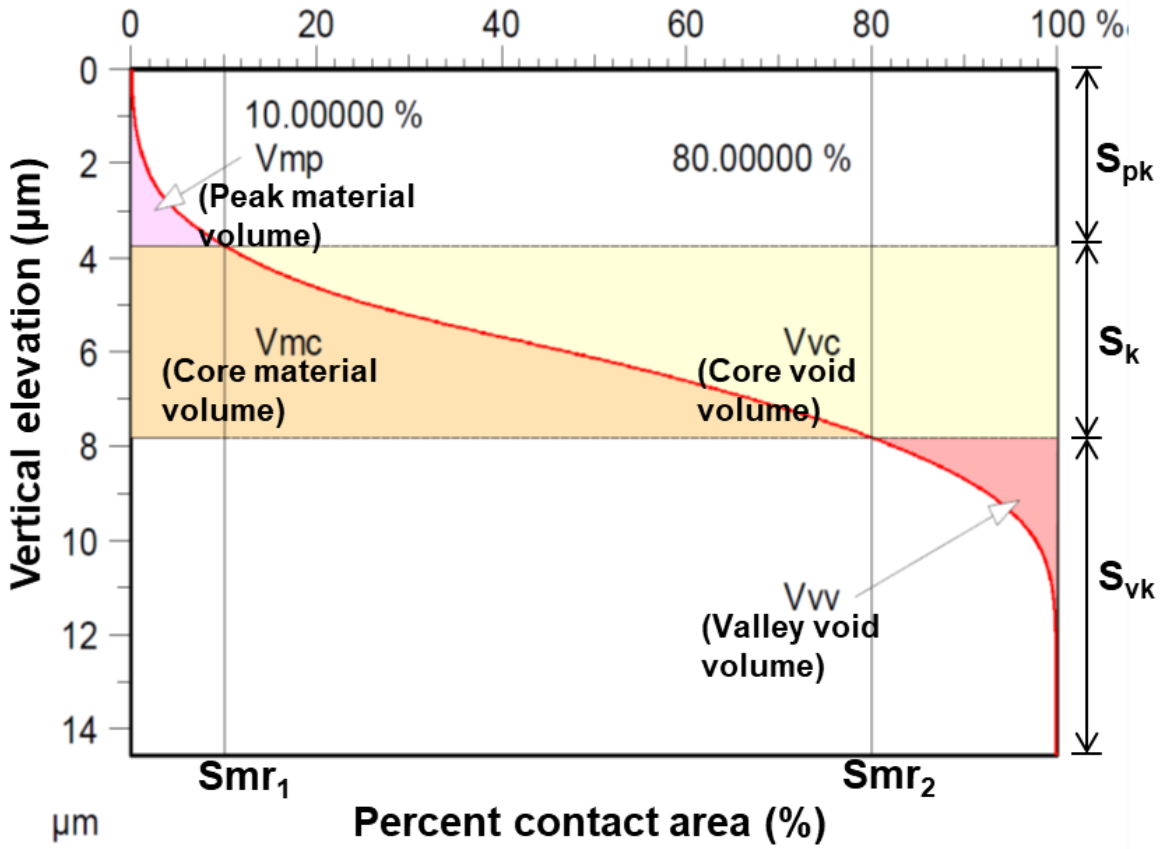

Fig. 1 : Material ratio curve obtained from white light interferometry.

Appendix - IV

Coefficient of friction of cemented carbide *(WC-15.6Co)*

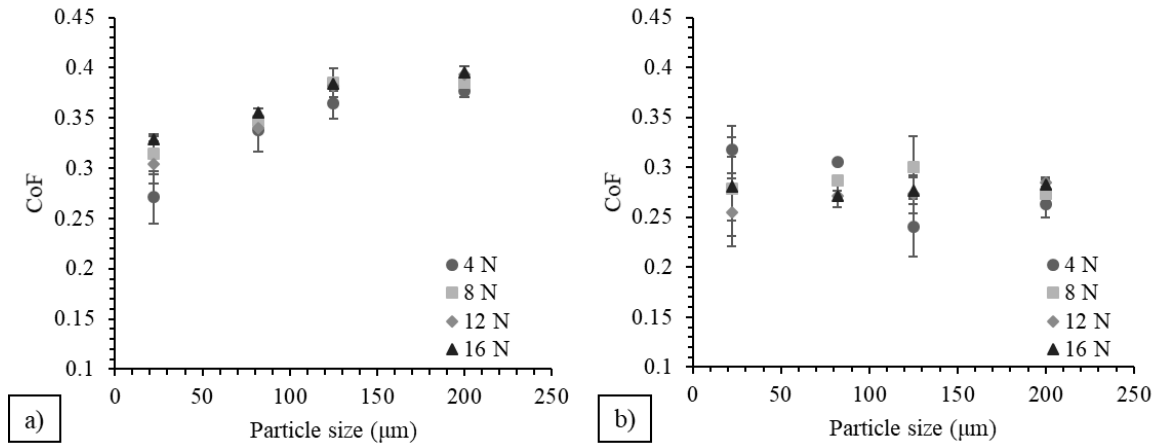

Fig. 2 – Friction coefficient vs load and particle size of WC-Co against (a) SiC and (b) Al_2O_3 abrasives.

Coefficient of friction of NbC-Ni cermet *($NbC-12Ni-10Mo_2C$)*

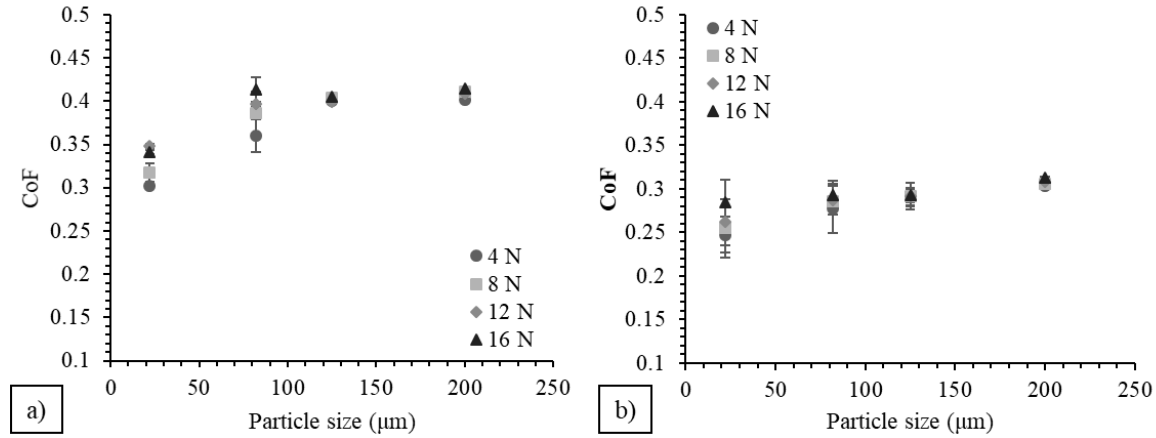

Fig. 3 – Friction coefficient vs load and particle size of NbC-Ni cermet against (a) SiC and (b) Al_2O_3 abrasives.